NORTH-HOLLAND

Dynamics of Coupled Nonlinear Maps and Its Application to Ecological Modeling

F. E. Udwadia and N. Raju

Department of Mechanical Engineering
430K Olin Hall
University of Southern California
Los Angeles, California 90089-1453

Transmitted by R. Kalaba

ABSTRACT

This paper investigates the behavior of coupled nonlinear dynamical systems. We take two such dynamical systems (or units), couple them together, and study the effect of coupling on the dynamics. We demonstrate that coupling two chaotic units can indeed stabilize both of them. Several results describing the global dynamics of the coupled nonlinear system are established. Using them, we show that, by-and-large, the presence of coupling appears to increase the orderliness of the coupled system's response, producing periodicity, synchronicity, and quasi-symmetry. Using exponential maps which are commonly used to simulate-population dynamics, we establish the applicability of our results to population dynamics. © *Elsevier Science Inc., 1997*

1. INTRODUCTION

Before Henri Poincaré's (1892) discovery of holonomic orbits, most people were not even aware of chaos. With the increasingly easier access to faster computation, we are now finding chaos in many computer simulations of natural processes. We come across chaos in the trajectories of planets. We find chaos in different classes of chemical reactions, not to mention turbulence in fluids. We encounter chaos in population dynamics. The number of systems which seem to behave chaotically indeed appears to be overwhelming.

APPLIED MATHEMATICS AND COMPUTATION 82:137–179 (1997)

655 Avenue of the Americas, New York, NY 10010
0096-3003/97/$17.00
PII S0096-3003(96)00027-6

If this tremendous amount of chaos were to grow unchecked, nothing in this world could be orderly. Yet, even untutored experience indicates that by and large there is considerable order in the physical world. This stark difference raises several questions. Why is there such stability despite all the reported chaos? What are the factors that contribute to such stability? How can stability be enhanced/destroyed?

There may be many reasons for the observed stability of physical systems present amidst all this reported chaos. In a given system there are several parameters and chaos may evince for only certain ranges of these parameters. If the probability that the system attains these ranges of parameters is small, then the probability of this system being chaotic is also small. However, estimating such probabilities may be difficult.

Further, in reality, most physical systems are coupled. To render them easy to study, many of the couplings present in physical systems are either eliminated or approximated. Therefore, another possibility is that a chaotic system becomes stable when coupled with other chaotic systems. Cast differently, can adding a "jug" of chaos to another "jug" of chaos lead to stability? For example, if one group (or species) that displays chaotic growth (in isolation) is coupled with another chaotically evolving group, could the resulting system exhibit orderly dynamical behavior? Could, for example, migratory coupling of two chaotically evolving insect populations stabilize these populations? In short, can the collective behavior of a system transcend that of its chaotic components? Our investigation demonstrates the possibility of such stabilization. Where complete stabilization is not possible, we find that there could be diagonal-attraction or synchronicity—the 'count' of both systems may eventually become identical even though they were different initially.

The nonlinear model used here to study the role of coupling in stabilizing and synchronizing nonlinear systems is derived from population dynamics.

The study of population dynamics in ecological systems has several applications. For example, it is of great concern whether fishermen can get a fairly uniform catch throughout the year. If the population trend of fish is erratic in a particular region, the fishermen may not be able catch any significant amount during some seasons, and it is important to analyze the factors contributing to such erratic behavior. Further, studying if the current population of a particular species is sufficient enough to sustain it, may play a crucial role in avoiding species extinction. In short, population bursts and population collapse have significant implications in understanding ecological systems.

Several mathematical models have been employed by different researchers to simulate population dynamics. The most common models employ nonlinear difference maps. These models describe the evolution of a

single species at a particular habitat. They assume that emigration and immigration are negligible. On the other hand, there are systems in which migration is significant enough to alter the population dynamics at the particular habitat [1]. However, there are not that many studies that analyze the effect of migration on population dynamics.

We analyze the effect of migration by studying the interactive dynamics of two subcolonies of a single species. The growth of a single subcolony is often modeled as a difference equation of the type

$$x_{n+1} = p(x_n). \tag{1}$$

Here x_n is the population size at time t_n, and the map p gives the size of the population at the next update in time, t_{n+1}. Exponential maps, wherein the function p is defined as

$$p(x) = xe^{r(1-x)} \tag{2}$$

are used extensively in the biological literature [2] to describe a population with a propensity to grow exponentially at low population densities and a tendency to decrease at high density. The nature of the nonlinear behavior is regulated by the growth parameter r. Ricker [2], based on empirical data, has postulated that exponential maps govern the population of a prey species if the predators, at any given abundance, consume a fixed fraction of the prey species, as though they were captured at random encounters. The same model also governs the population dynamics of a single species of organisms which is regulated by an epidemic disease at high population densities.

The system described by equations (1) and (2) shows complicated dynamics. May [3] provides some of the salient features of this map as the parameter r is gradually varied. Starting from a low value of the growth parameter r, the fixed point of the map becomes unstable when r reaches a value of 2 (Figure 1). The point of accumulation of cycles of period 2^n occurs when $r \simeq 2.6924$, and the 3-period cycle appears at $r \simeq 3.1024$. Beyond this value of r, the system exhibits chaotic behavior interspersed by thin periodic bands. The chaotic or periodic behavior of the system is reflected in the positive or negative values for the Lyapunov exponent plotted in Figure 1.

In this paper we consider two interacting populations (colonies) of biological organisms, each of whose population dynamics is described by (1) and (2). The interaction between these colonies may be thought of as being brought about by migration between the two populations. We shall deal

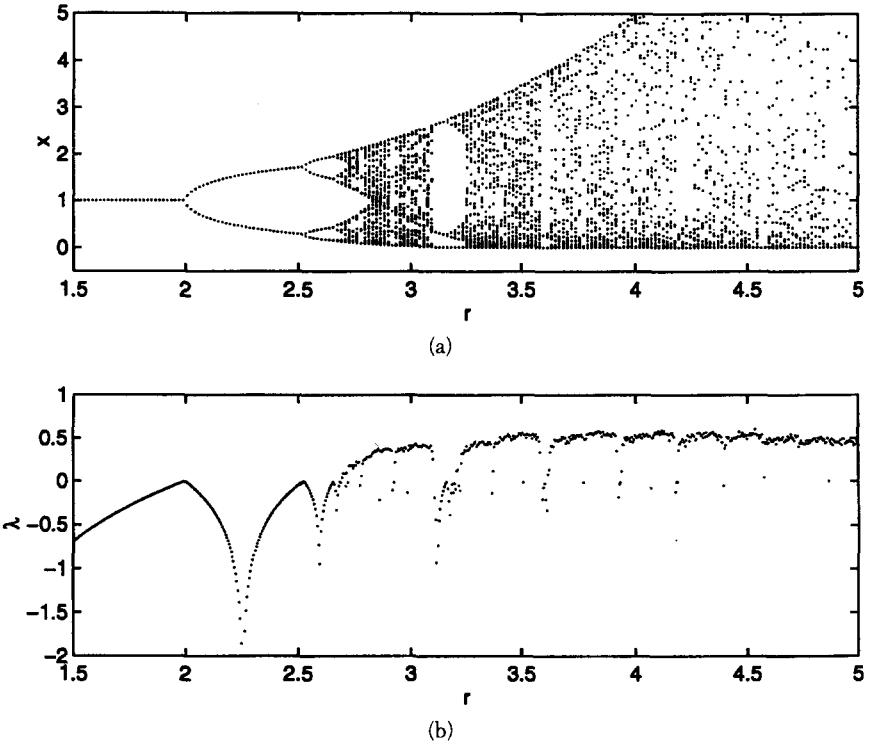

FIG. 1. (a) Bifurcation diagram and (b) Lyapunov exponent plotted against r for an uncoupled exponential map. The accumulation point occurs at $r \simeq 2.6924$.

with two separate situations: the first when each population has the same growth parameter and the second when the two populations have different growth parameters. The first situation is likely to arise, when the two populations occupy environmental niches of habitat which are equal in most respects.

The similar case of coupled logistic maps has been analyzed by Gyllenberg et al. [4] to study the effect of migration on population dynamics. They have presented a detailed analysis of fixed points and two-periodic orbits. Coupled logistic equations with different forms of coupling have been investigated by, among others, Chowdhury and Chowdhury [5] and Kaneko [6].

Our aim is to investigate the stable and chaotic dynamics of the coupled system. The effect of coupling on the system dynamics is investigated in detail. *It is demonstrated that coupling has a stabilizing effect.* Wherever

possible we present analytical results. Where such analytical results could not be obtained we show numerical computations to understand the behavior of the coupled system. The model is introduced in Section 2. Section 3 analyzes the interactive dynamics that transpires in the system. And our conclusions and discussions are presented in Section 4.

2. THE MODEL

We consider two interacting populations denoted by x and y of two colonies of the same species of organisms. Assuming that the populations grow as per the exponential map, the population in the first location at the end of one time period (say, one year) is $x\exp[r_x(1-x)]$ while that at the second location is $y\exp[r_y(1-y)]$. Further, if only fraction d of the population remains at the same location while the rest emigrate to the other location, we can arrive at the following equation governing the two populations x and y

$$x_{n+1} = dx_n \exp[r_x(1-x_n)] + (1-d)\, y_n \exp[r_y(1-y_n)] \tag{3}$$

$$y_{n+1} = (1-d)\, x_n \exp[r_x(1-x_n)] + dy_n \exp[r_y(1-y_n)]$$

where, as usual, the subscript n denotes the time t_n. The growth rates for the two subcolonies are given by r_x and r_y. The parameter d describes the extent of coupling between the two populations. When $d = 1$, the two populations evolve in time independently of each other; we have two uncoupled maps each describing the population count of one colony at any time t_n. On the other hand, when $d = 0$, the populations are most intensely coupled, the entire population produced at one location migrates to the other. When $0 \leqslant d < 1$, the two colonies interact with each other. The coupling used here is symmetric, i.e., the percentage migrating from one location is the same as that migrating from the other. Such a symmetry reduces the number of parameters in the problem. We shall sometimes denote the mapping described by equation (3), for brevity, as

$$(x_{n+1}, y_{n+1}) = M(r_x, r_y, d) \circ (x_n, y_n), \tag{4}$$

to explicitly indicate the dependence on the triplet of parameters (r_x, r_y, d). Before describing the dynamical behavior of the coupled map in the ensuing sections, we would like to point out that many of the following results are independent of the functional form of the map M.

3. DYNAMICAL BEHAVIOR

In subsection 3.1 several analytical results, some dealing with the global dynamics, are presented. Further dynamical characteristics of the system are explored numerically in subsections 3.2 and 3.3. Subsection 3.2 focuses on the symmetrical case $r_x = r_y = \hat{r}$. Subsection 3.3 aims at investigating the asymmetric case $r_x \neq r_y$.

3.1. Analytical Results

RESULT 1. Consider the orbits of the map (4) for a specific set of parameters $r_x = \hat{r}_x$, $r_y = \hat{r}_y$, and $d = \hat{d}$. For each orbit of the map (4) described by $\{(\hat{x}_n, \hat{y}_n) \mid n = 0, 1, 2, ., ...\}$ for a given triplet $(\hat{r}_x, \hat{r}_y, \hat{d})$ of parameter values, there corresponds an orbit described by $\{(\hat{y}_n, \hat{x}_n) \mid n = 0, 1, 2, ., ...\}$ for the parameter triplet $(\hat{r}_y, \hat{r}_x, \hat{d})$.

PROOF. This result is obvious from equations (3) since the interchanges

$$\left.\begin{array}{l} x_n \to y_n \\ y_n \to x_n \\ \hat{r}_x \to \hat{r}_y \\ \hat{r}_y \to \hat{r}_x \end{array}\right\} \Rightarrow \left\{\begin{array}{l} x_{n+1} \to y_{n+1} \\ y_{n+1} \to x_{n+1} \end{array}\right\}. \qquad \square$$

RESULT 2. When $r_x = r_y = \hat{r}$, for each orbit $\{(\hat{x}_n, \hat{y}_n) \mid n = 0, 1, 2, ., ...\}$, corresponding to the parameter values $(\hat{r}, \hat{d})$ corresponds an orbit $\{(\hat{y}_n, \hat{x}_n) \mid n = 0, 1, 2, ., ...\}$.

PROOF. The result follows directly from Result 1 by setting $r_x = r_y = \hat{r}$. $\square$

COROLLARY 1. *When $r_x = r_y = \hat{r}$, for each n-periodic orbit of the map* (3) *described by* $\{(\hat{x}_n, \hat{y}_n) \mid n = 0, 1, 2, ., ...\}$ *corresponding to a set of parameters* $(\hat{r}, \hat{d})$, *there exists another n-periodic orbit described by* $\{(\hat{y}_n, \hat{x}_n) \mid n = 0, 1, 2, ., ...\}$.

PROOF. The result is a special case of Result 2 when the orbits are periodic. □

RESULT 3. Consider the orbit $\{(\hat{x}_n, \hat{y}_n) \mid n = 0, 1, 2, ., \ldots\}$ corresponding to a certain value of the parameter $d = 1/2 - d_0, 0 \leqslant d_0 \leqslant 1/2$, with $r_x = r_y = \hat{r}$. For each such orbit, there corresponds an orbit given by $\{(\hat{x}_0, \hat{y}_0), (\hat{y}_1, \hat{x}_1), (\hat{x}_2, \hat{y}_2), (\hat{y}_3, \hat{x}_3), \ldots\}$, corresponding to the parameter $d = 1/2 + d_0$, with $r_x = r_y = \hat{r}$, i.e., each alternate point of the second orbit has its x- and y-coordinate switched with respect to the corresponding point of the first orbit.

PROOF. The result follows from the observation that for an initial point $(\hat{x}_n, \hat{y}_n)$, if

$$(\hat{x}_{n+1}, \hat{y}_{n+1}) = M(\hat{r}, \hat{r}, 1/2 - d_0) \circ (\hat{x}_n, \hat{y}_n), \tag{5}$$

then,

$$(\tilde{x}_{n+1}, \tilde{y}_{n+1}) = M(\hat{r}, \hat{r}, 1/2 + d_0) \circ (\hat{x}_n, \hat{y}_n) = (\hat{y}_{n+1}, \hat{x}_{n+1}). \tag{6}$$

Furthermore, denoting,

$$(\hat{x}_{n+2}, \hat{y}_{n+2}) = M(\hat{r}, \hat{r}, 1/2 - d_0) \circ (\hat{x}_{n+1}, \hat{y}_{n+1}), \tag{7}$$

we find that

$$(\tilde{x}_{n+2}, \tilde{y}_{n+2}) = M(\hat{r}, \hat{r}, 1/2 + d_0) \circ (\tilde{x}_{n+1}, \tilde{y}_{n+1}) = (\hat{x}_{n+2}, \hat{y}_{n+2}) \tag{8}$$

and hence, the result.

COROLLARY 2. *If the map* $M(\hat{r}, \hat{r}, 1/2 - d_0)$, $0 \leqslant d_0 \leqslant 1/2$ *has a* $2n$*-period orbit starting from some* (x_0, y_0), $n = 1, 2, \ldots$, *then the map* $M(\hat{r}, \hat{r}, 1/2 + d_0)$ *must have a* $2n$*-period starting from the same point* (x_0, y_0), $n = 1, 2, \ldots$.

PROOF. This again is obvious from Result 3. □

COROLLARY 3. *If the map* $M(\hat{r}, \hat{r}, 1/2 - d_0)$, $0 \leqslant d_0 \leqslant 1/2$ *has a* $(2n - 1)$*-period orbit starting some* (x_0, y_0), $n = 1, 2, \ldots$, *with* $x_0 \neq y_0$, *then the map* $M(\hat{r}, \hat{r}, 1/2 + d_0)$ *must have a* $2(2n - 1)$*-period starting from the same point* (x_0, y_0), $n = 1, 2, \ldots$.

PROOF. This again is obvious from Result 3. □

As we shall see from numerical simulations, this property of the map yields a sort of quasi-symmetry to the bifurcation plots of the orbits with respect to the parameter d.

RESULT 4. For $r_x = r_y = \hat{r}$ the orbit of map (4) starting with (x_0, x_0) will always consist of points of the form (x_n, x_n). In other words, orbits which begin on the diagonal in the (x, y) phase space lie entirely on the diagonal.

PROOF. This follows from the observation that

$$(x_{n+1}, x_{n+1}) = M(\hat{r}, \hat{r}, d) \circ (x_n, x_n). \tag{9}$$

□

The above result indicates that for orbits that begin on the diagonal in the phase space, each state of the dynamical system behaves as if it were governed by a single exponential map of the form of (2).

RESULT 5. For $d = 1/2$ the orbit of the map (4) starting with (x_0, y_0) will consist of points of the form (x_n, x_n) for all values of r_x and r_y after the first iteration.

PROOF. This result is obvious from the observation that the map (4) redistributes the total population equally among the two locations. □

We now consider the fixed points of the map (4). It is easily seen that the points $(0, 0)$ and $(1, 1)$ are fixed points.

RESULT 6. The fixed point $(0, 0)$ of the map $M(r_x, r_y, d)$ is unstable for all $r_x, r_y > 0$ and $0 \leqslant d \leqslant 1$.

PROOF. The Jacobian matrix of the map $M(r_x, r_y, d)$ evaluated at (x, y) is given by

$$J(x, y) = \begin{bmatrix} d(1 - xr_x)\exp[r_x(1 - x)] & (1 - d)(1 - yr_y)\exp[r_y(1 - y)] \\ (1 - d)(1 - xr_x)\exp[r_x(1 - x)] & d(1 - yr_y)\exp[r_y(1 - y)] \end{bmatrix}. \tag{10}$$

Hence,

$$J(0, 0) = \begin{bmatrix} d\exp(r_x) & (1 - d)\exp(r_y) \\ (1 - d)\exp(r_x) & d\exp(r_y) \end{bmatrix}, \tag{11}$$

and thus, for $(0, 0)$ to be stable we require, using the usual determinant-trace criterion of the Jacobian matrix, that

$$(2d - 1)\exp(r_x + r_y) < 1, \tag{12}$$

and

$$(2d - 1)\exp(r_x + r_y) \pm d\left[\exp(r_x) + \exp(r_y)\right] + 1 > 0. \tag{13}$$

For condition (12) to be true

$$d < \frac{1}{2} + \frac{1}{2\exp(r_x + r_y)}.$$

Let

$$d = \frac{1}{2} + \frac{1}{2\exp(r_x + r_y)} - \epsilon.$$

To satisfy condition (13),

$$2 - 2\epsilon \exp(r_x + r_y) - \left[\exp(r_x) + \exp(r_y)\right] > 0$$

which cannot be satisfied for any positive values for r_x and r_y. Hence the result. □

RESULT 7. The fixed point $(1, 1)$ is stable when

$$(1 - r_x)(1 - r_y)(2d - 1) < 1, \tag{14}$$

and

$$(1 - r_x)(1 - r_y)(2d - 1) \pm d(2 - r_x - r_y) + 1 > 0. \tag{15}$$

PROOF. The result is obvious by evaluating the Jacobian matrix given by equation (10) at $(1, 1)$. □

Figure (2) shows the region in the parameter space r_x, r_y, and d in which the fixed point $(1, 1)$ is stable. The region enclosed by the surface plots show the stable regime in both the subplots. When $r_x = r_y = \hat{r}$, equations (14) and (15) simplify and it can be shown that for $\hat{r} < 2$, the fixed point $(1, 1)$ is stable for all $0 \leqslant d \leqslant 1$.

Besides these two fixed points which occur for all values of the triplet (r_x, r_y, d) there are other fixed points whose coordinates depend on specific values of the triplet.

RESULT 8. A fixed point (x_i, y_i) of the map $M(r_x, r_y, d)$ must satisfy the condition

$$\frac{r_x - \ln(1 - dq) + \ln[d + (1 - 2d)]}{r_x[r_y - \ln(q)]} = \frac{d + (1 - 2d)q}{r_y(1 - d)} \tag{16}$$

$$q = e^{r_y(1 - y_i)} \qquad \text{and} \qquad x_i = y_i \frac{d + (1 - 2d)q}{1 - d}.$$

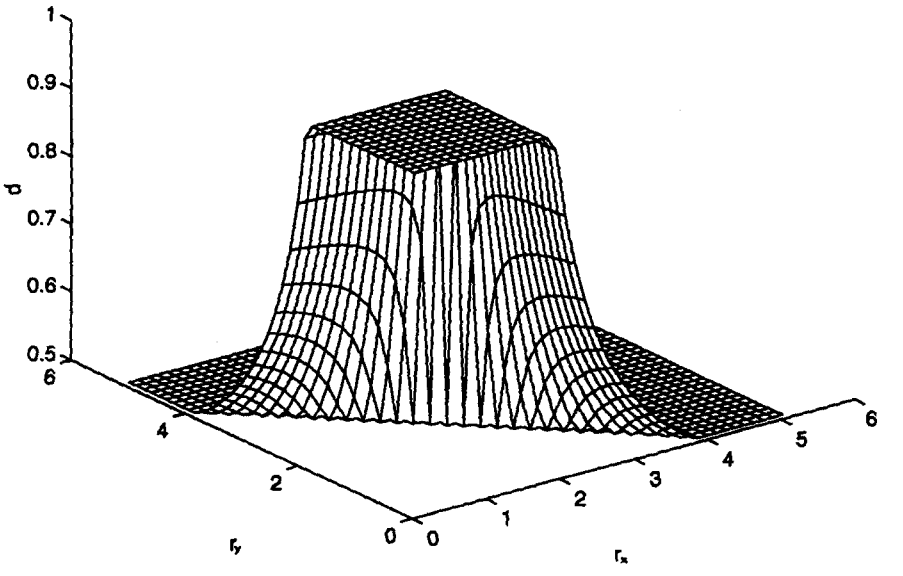

(a)

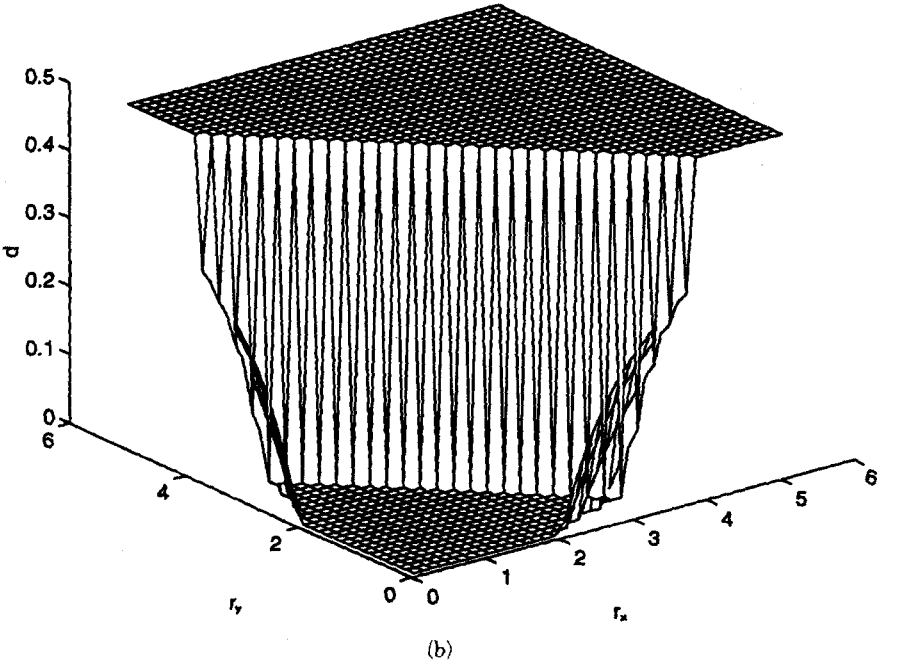

(b)

FIG. 2. The stability of the fixed point at (1, 1). If the point marked by the triplet (r_x, r_y, d) falls inside the volume under the shaded surface, then the fixed point (1, 1) is stable.

When $r_x = r_y = \hat{r}$, this equation simplifies to

$$\frac{\hat{r} - \ln(1 - dq) + \ln[d + (1 - 2d)]}{\hat{r}[\hat{r} - \ln(q)]} = \frac{d + (1 - 2d)q}{\hat{r}(1 - d)}. \quad (17)$$

PROOF. The result follows directly from the definition of the map. □

Figure (3) shows both the stable and the unstable fixed points for three values of $\hat{r}$. Notice that the stable fixed points arise for values of $d < 0.18$, indicating that one period orbits of the coupled system occur only in the

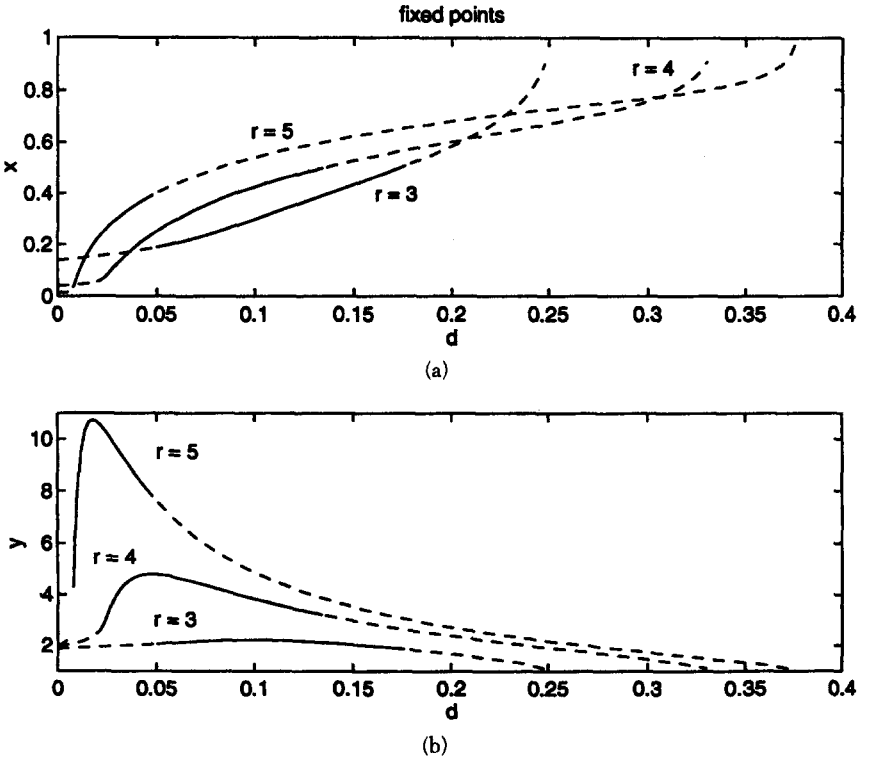

FIG. 3. (a) x-coordinate and (b) y-coordinate of the fixed points plotted against the coupling parameter d. Fixed points marked by solid lines are stable while those marked by dashed lines are unstable.

presence of strong coupling between the two colonies. In addition to the plotted points there are other stable fixed points, which by Corollary 1 can be obtained by interchanging the two ordinates x and y. The unstable fixed points are also plotted on Figure 3. Again, another set of unstable fixed points can be obtained by flipping the two ordinates.

Next we consider some properties of the Lyapunov Exponents λ_i,

$$\lambda_i = \lim_{n \to \infty} \frac{\log_e [|\mu_i|]}{n}, \quad i = 1, 2, \tag{18}$$

where μ_i are the two eigenvalues of the matrix produced by multiplying the Jacobian matrices at every successive iteration.

RESULT 9. The Lyapunov exponents of the map $M(\hat{r}, \hat{r}, 1/2 - d_0)$, $0 \leqslant d_0 \leqslant 1/2$ starting from some (x_0, y_0) are the same as that of the map $M(\hat{r}, \hat{r}, 1/2 + d_0)$ starting from the same point (x_0, y_0).

PROOF. Let

$$M(\hat{r}, \hat{r}, 1/2 - d_0) \circ (x_n, y_n) = (x_{n+1}, y_{n+1}). \tag{19}$$

By Result 3,

$$M(\hat{r}, \hat{r}, 1/2 + d_0) \circ (x_n, y_n) = (\tilde{x}_{n+1}, \tilde{y}_{n+1}) = (y_{n+1}, x_{n+1}) \tag{20}$$

and

$$\begin{aligned} M(\hat{r}, \hat{r}, 1/2 - d_0) \circ (x_{n+1}, y_{n+1}) &= M(\hat{r}, \hat{r}, 1/2 + d_0) \circ (\tilde{x}_{n+1}, \tilde{y}_{n+1}) \\ &= (x_{n+2}, y_{n+2}). \end{aligned} \tag{21}$$

By (10), the Jacobian matrix for these two system at every iteration is of the form

$$J_n\big[M(\hat{r}, \hat{r}, 1/2 - d_0)\big]_{(x_n, y_n)} = \begin{bmatrix} a_{11} & a_{12} \\ a_{21} & a_{22} \end{bmatrix} \tag{22}$$

$$\tilde{J}_n\big[M(\hat{r}, \hat{r}, 1/2 + d_0)\big]_{(\tilde{x}_n, \tilde{y}_n)} = \tilde{J}_n\big[M(\hat{r}, \hat{r}, 1/2 + d_0)\big]_{(x_n, y_n)}$$

$$= \begin{bmatrix} a_{21} & a_{22} \\ a_{11} & a_{12} \end{bmatrix} \tag{23}$$

$$J_{n+1}\big[M(\hat{r}, \hat{r}, 1/2 + d_0)\big]_{(x_{n+1}, y_{n+1})} = \begin{bmatrix} b_{11} & b_{12} \\ b_{21} & b_{22} \end{bmatrix} \tag{24}$$

$$\tilde{J}_{n+1}\big[M(\hat{r}, \hat{r}, 1/2 + d_0)\big]_{(\tilde{x}_{n+1}, \tilde{y}_{n+1})} = \tilde{J}_{n+1}\big[M(\hat{r}, \hat{r}, 1/2 + d_0)\big]_{(y_{n+1}, x_{n+1})}$$

$$= \begin{bmatrix} b_{12} & b_{11} \\ b_{22} & b_{21} \end{bmatrix}. \tag{25}$$

Hence, it is seen that

$$J_{n+1} J_n = \tilde{J}_{n+1} \tilde{J}_n. \tag{26}$$

Therefore, the eigenvalues and the Lyapunov exponents are symmetric about $d = 1/2$. □

RESULT 10. When $d = 1/2$, one Lyapunov exponent tends to $-\infty$.

PROOF. On setting $d = 1/2$ in (10) the determinant vanishes and hence the result. □

We would like to reiterate that results 2 to 5, 9, 10, and their corollaries are independent of the functional form of the maps chosen.

3.2. Global Characterization of Dynamics and Numerical Results for the Symmetric Case

This section is devoted to studying the effect of migration (or coupling) when the growth rates of the two interacting colonies are identical i.e., $r_x = r_y = \hat{r}$. Now the governing system expressed by (3) has only two parameters, $\hat{r}$, and d. The parameter d can vary from zero to unity. The parameter $\hat{r}$ can be any positive real number. We consider cases in which $\hat{r} \leqslant 5$ because for higher values of $\hat{r}$ the exponential term can cause unrealistically large fluctuations. We shall refer to the state (chaotic or periodic) of each of the maps in isolation as their base state. Because the two maps are identical ($r_x = r_y$) they are characterized by the same base state. First we consider values of $\hat{r}$ for which the base state plotted in Figure 1 is chaotic say, $r = 3$.

We begin with a description of the bifurcation plots. To arrive at the bifurcation plots of the coupled system we first apply the map 5000 times iteratively on an initial condition not on the diagonal ($x_0 \neq y_0$). The x and y coordinates are then obtained by iterating another hundred times. This procedure is repeated for several values of d and $\hat{r}$. The resulting values of x and y at every iteration for three representative values of $\hat{r} (= 3, 4, 5)$ are plotted against d in Figures (4) and (5), respectively. For the three values of $\hat{r}$ chosen, the underlying single map described by (2) is chaotic (Figure 1). Upon coupling two such maps, a variety of dynamical behaviors emerge depending on the extent of coupling. Yet the gross dynamics can broadly be described as follows.

(1) There is a quasi-symmetry about $d = 1/2$, i.e., the dynamical behavior when $d = 1/2 + k$ is very similar to that when $d = 1/2 - k$, $0 \leqslant k \leqslant 1/2$. As a result, the dynamics in zones V, VI, and VII are similar to those of zones III, II, and I, respectively. (2) The behavior can be categorized into seven zones. (3) Zone I is a region of complex dynamics. This mostly chaotic region does have several periodic orbits. Similar behavior is observed in zone VII, the symmetric equivalent of zone I. (4) Zone II is characterized by periodic behavior. Similarly, its symmetric equivalent, zone VI, is periodic. (5) Completely chaotic behavior is observed in both zone III and zone V. (6) Zone IV is chaotic but synchronous i.e., both the populations are identical in size. This synchronicity is *not* readily visible in Figure 4 and 5. We need to perform a coordinate transformation, to identify the synchronicity as discussed later in Figure 9. First we consider zone I.

The dynamical behavior in zone I is complicated. This region is mostly chaotic with a few periodic orbits embedded in between. Similarly, by virtue of the quasi-symmetry about $d = 1/2$, zone VII is mostly chaotic although some multiperiod trajectories are observed. There are however, some differences between zones I and VII, for instance, the periodicity of some periodic

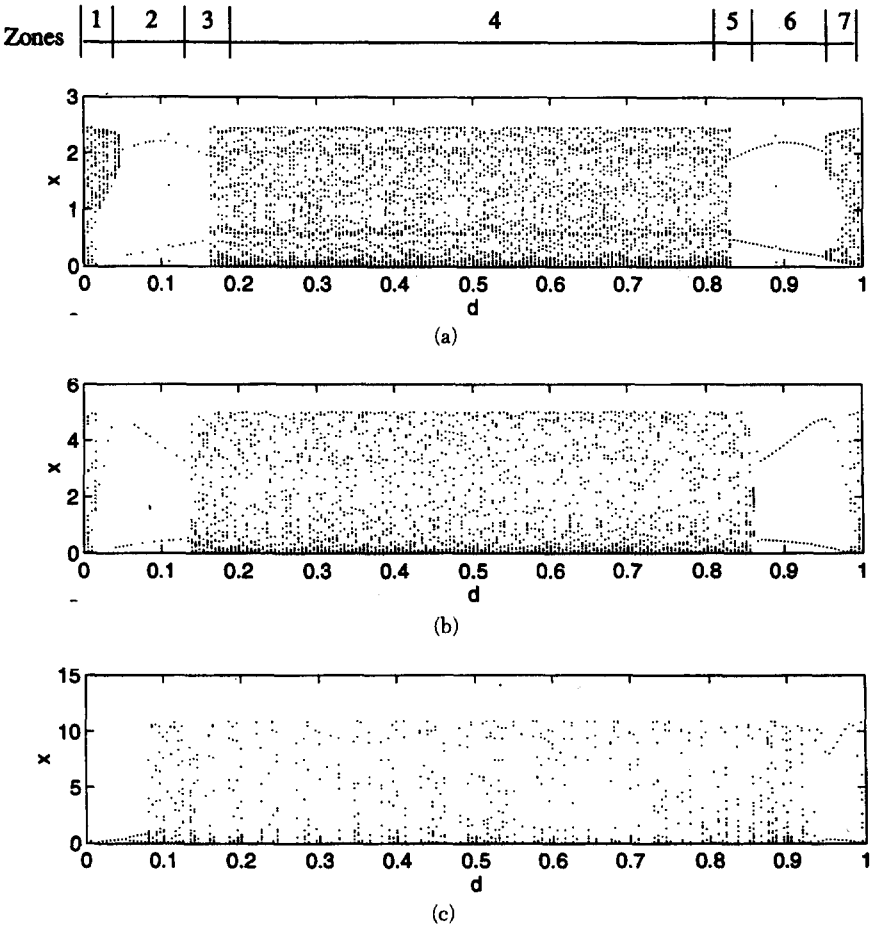

FIG. 4. Bifurcation diagrams depicting the x-ordinates against d. (a) $\hat{r} = 3$; (b) $\hat{r} = 4$; (c) $\hat{r} = 5$. The underlying single map is chaotic for all these three values of r. Zone II and zone VI are periodic. Thus, by choosing an appropriate coupling one can stabilize chaotic systems. Zone markings refer to regimes in b. Similar qualitative zones are present for Figures a and c.

orbits may be different. Let us consider an odd period orbit in zone I (Figure 6a). The equivalent orbit in zone VII can be obtained by reflecting d about one-half. The periodicity of this equivalent orbit is doubled in agreement with Corollary 3. The five-period orbit in zone I (Figure 6a) becomes a ten-period orbit in zone VII (Figure 6b). The five additional points on this ten-period orbit can be obtained by transposing the x and y coordinates of

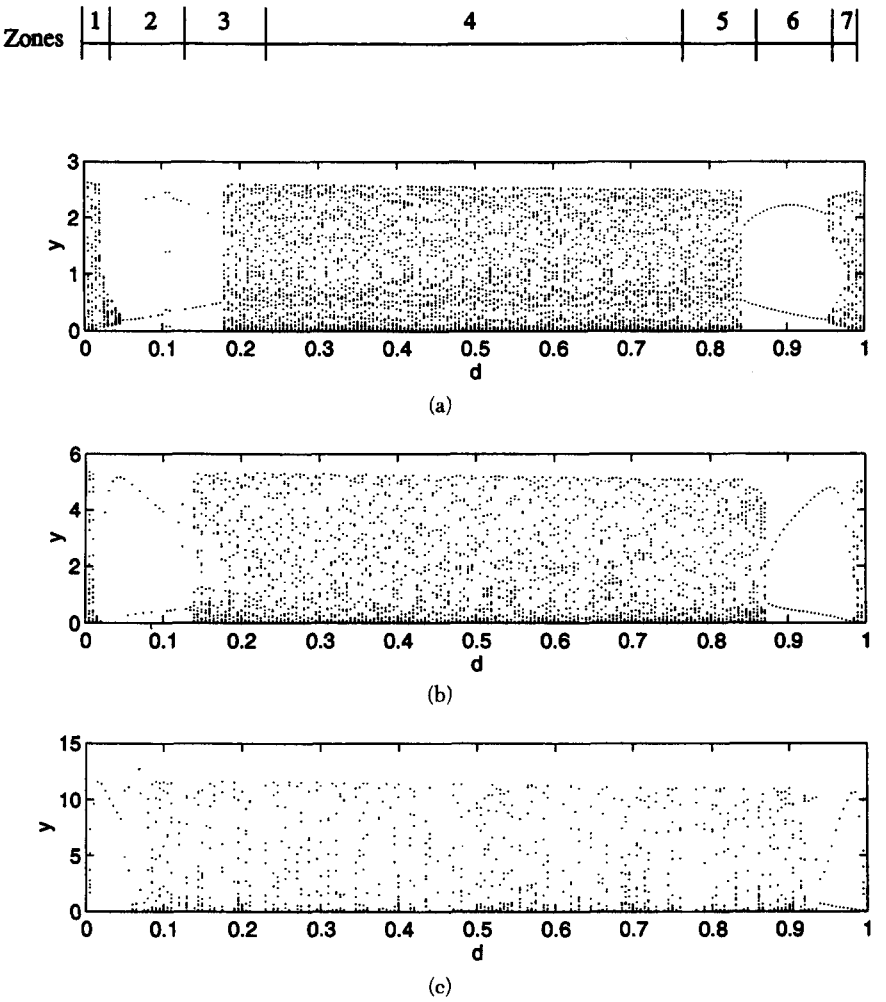

FIG. 5. Bifurcation diagrams depicting the y-ordinates against d. (a) $\hat{r} = 3$; (b) $\hat{r} = 4$; (c) $\hat{r} = 5$. Zone markings refer to regimes in Figure b. Similar qualitative zones are present for Figures a and c.

the five points in the five-period orbit of zone I. On the other hand, even period orbits have the same periodicity in both these zones are required by corollary 2. The ten-period orbit in zone I remains as a ten-period orbit in zone VII (shown later in Figures 6c and d). However, the x and y coordinates of alternate points on an even-period orbit in zone VII are

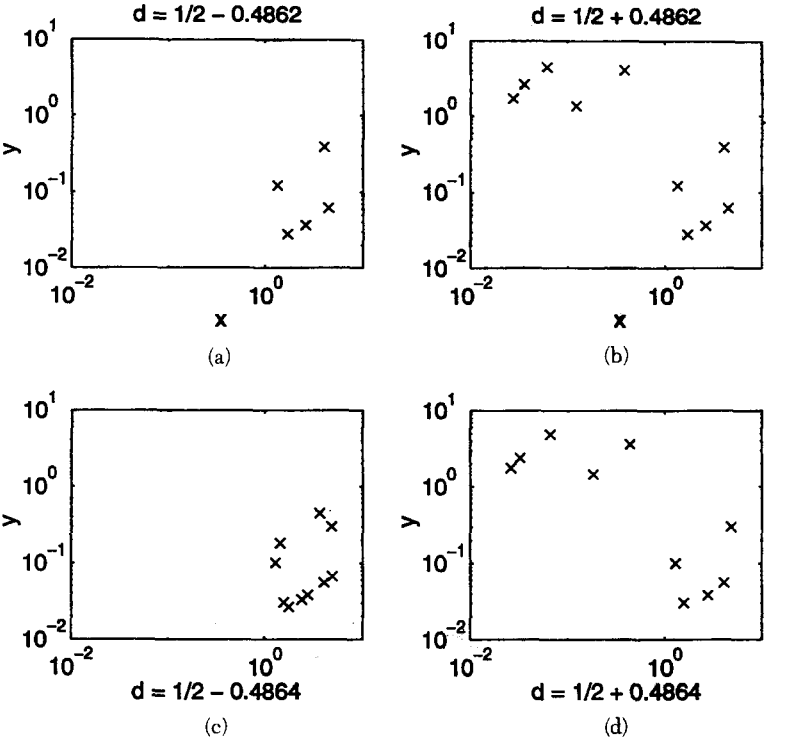

FIG. 6. (a) A five-period orbit in zone 1. The corresponding orbit in zone VII (obtained by reflecting d about $1/2$) has a period of ten as in (b). (c) A ten-period orbit in zone I. The corresponding orbit in zone VII remains ten-periodic as in (d). Thus, odd-period orbits in zone I double in periodicity when reflected about $d = 1/2$ while even-period orbits maintain the same period when reflected about $d = 1/2$. $\hat{r} = 4$.

different from those of the equivalent orbit in zone I; in fact, these differing points in zone VII can be obtained by interchanging the x and y values of the corresponding points in zone I. Such a transposition of coordinates is furthermore in agreement with Result 3. Thus, the dynamical behavior is quasi-symmetric about $d = 1/2$.

The periodic zone II can be further divided into two subzones IIA and IIB (see Figure 7). Subzone IIA is characterized by stable 1-period orbits corresponding to the stable fixed points of Figure (3). For a first look, the trajectories on the bifurcation plots (4) and (5) may appear to be 2-period orbits. But they are actually, in agreement with Corollary 1, two separate 1-period orbits. Both these 1-period orbits, obtainable from (17), are symmetric about the diagonal $x = y$, i.e., one 1-period orbit can be obtained by

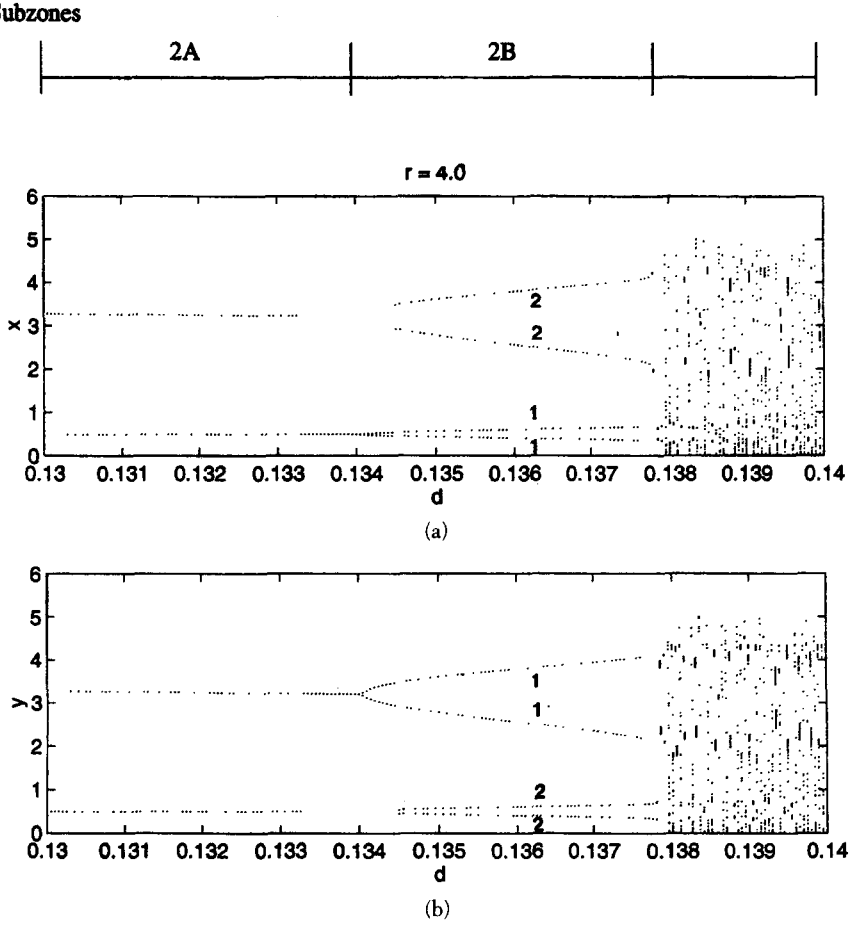

FIG. 7. (a) Zone II of Figure 4b enlarged. (b) Zone II of Figure 5b enlarged. The one-period orbits bifurcate into two-period orbits via a pitchfork bifurcation. The transition from the two-period orbits to chaos is sudden.

interchanging the coordinates of the other. A 1-period orbit means that the dynamics is in *complete equilibrium*. In other words, *by coupling two chaotic units one can arrive at a system which is in equilibrium*. The second subzone IIB is characterized by two distinct 2-period orbits. For $r = 5$ one of these 2-period orbits is clearly visible in Figures 4 and 5. For $r = 4$, both the 2-period orbits can be observed by enlarging the region around $d = 0.13$ (Figure 7). The transition from subzone IIA to subzone IIB is marked by a pitchfork bifurcation.

The dynamics in zone VI is also periodic and can be further divided into subzones VIC and VID (see Figure 8). Subzone VID, the symmetric equivalent of subzone IIA, is actually characterized by a single two-period orbit instead of the two 1-period orbits in subzone IIA (Figure 8). Cast differently, in zone VI the equivalent orbit of an odd-period orbit in zone II doubles its periodicity (as analytically proved in Corollary 3). Subzone VIC has two 2-period orbits similar to the orbits in subzone IIB. But the points traced by each of the two branches in subzone VIC (marked on Figure 8) are different

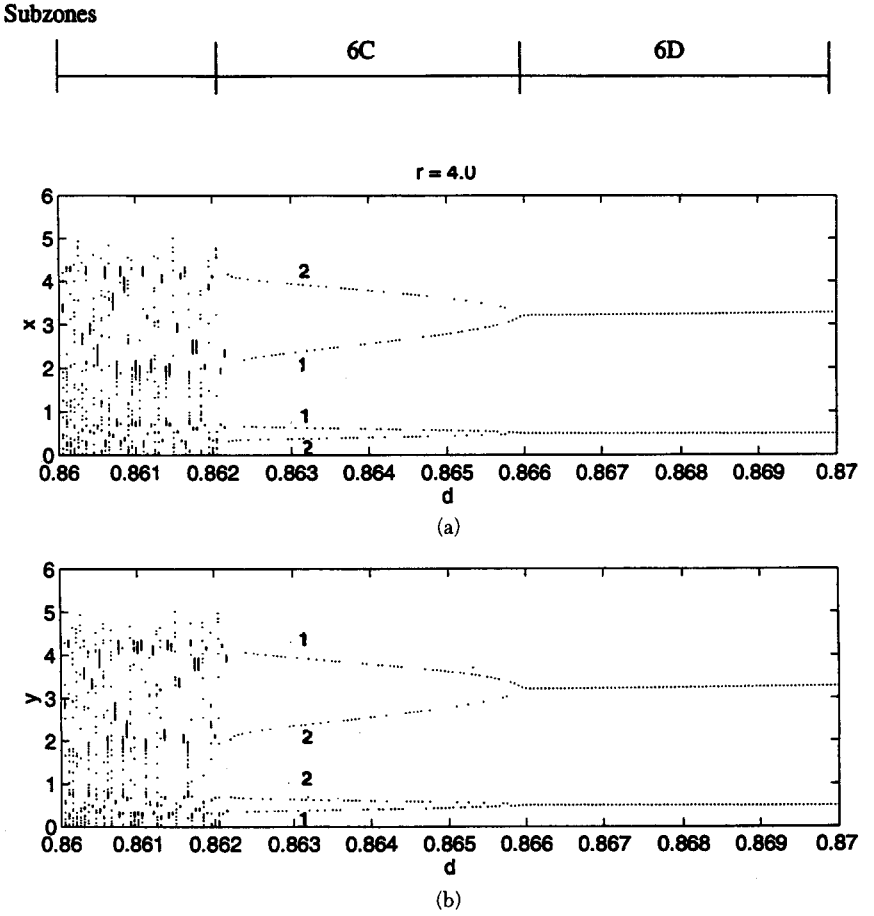

FIG. 8. (a) Zone VI of Figure 4b enlarged. (b) Zone VI of Figure 5b enlarged. The two-period orbit in subzone D bifurcates into a pair of two-period orbits. The transition from the two-period orbit to chaos is sudden.

from those in subzone IIB (marked on Figure 7). Overall, the behavior of one- and two-period orbits in zones II and VII are similar to the behavior of odd- and even-period orbits in zones I and VII.

Zone III is characterized by chaotic behavior. There is no visible structure in the dynamics of this zone. The same trend is observed in zone V as well.

Zone IV is chaotic but synchronous. Two populations are synchronous if their size are the same at every iteration. Therefore, their difference plotted in Figure 9 should be identically zero. Thus, we need to perform a coordinate transformation to $\xi = x - y$ and $\eta = x + y$. As seen in Figure 9, the range of d over which the populations are synchronous decreases as r is increased from 3 to 4 but increases as r is increased from 4 to 5. For all values r, this range of d is quite large. Hence, there is a significant probability that coupling can synchronize two units which in isolation behave chaotically. Similar synchronized motion has been observed in [7–9].

We next consider the transition from periodic behavior in zone II to chaotic behavior in either zone I or zone III. The boundary between zone I and II is marked by a Hopf bifurcation. This Hopf-bifurcation route to chaos is similar to that proposed by Ruelle and Takens [10]. Accordingly, the eigenvalues approach the unit circle as a pair of complex conjugates. The resulting closed loop trajectory is plotted in Figure 10a. The transition from zone VI to VII is also through a Hopf-bifurcation of the 2-period orbit. The resulting trajectory has two closed loops (Fig. 10b), and the orbit alternates between these two loops at every successive iteration.

The transition from Zone II to III is sudden. We investigated this region in fine detail with increments of d ranging from 10^{-9} to 10^{-2} and found no period-doubling process for all the three values of $\hat{r}$. For the particular value of $\hat{r} = 4$, explosive chaos occurs when $d = 0.13777076$. This transition is similar to the intermittency discussed by Pomeau and Manneville [11] and Udwadia and Guttalu [12].

In short, there are several interesting dynamics present in the coupled system. In particular there is a large range of the coupling parameter d over which dynamics of both units are synchronous. There is also a significant range over which the behavior is periodic.

So far we have investigated the dynamical behavior arising from one particular initial condition. It is of interest to investigate the effect of the particular initial conditions on the periodic, synchronous, and asynchronous trajectories produced. For initial conditions on the diagonal, by result 4, the orbit remains on the diagonal but is chaotic. However, for most of the other initial conditions the trajectories remains qualitatively the same as the ones described in figures (4) to (8). In particular, an n-periodic orbit remains n-periodic and a synchronous orbit remains synchronous for almost all initial conditions not on the diagonal. Recall that by Corollary 1, every

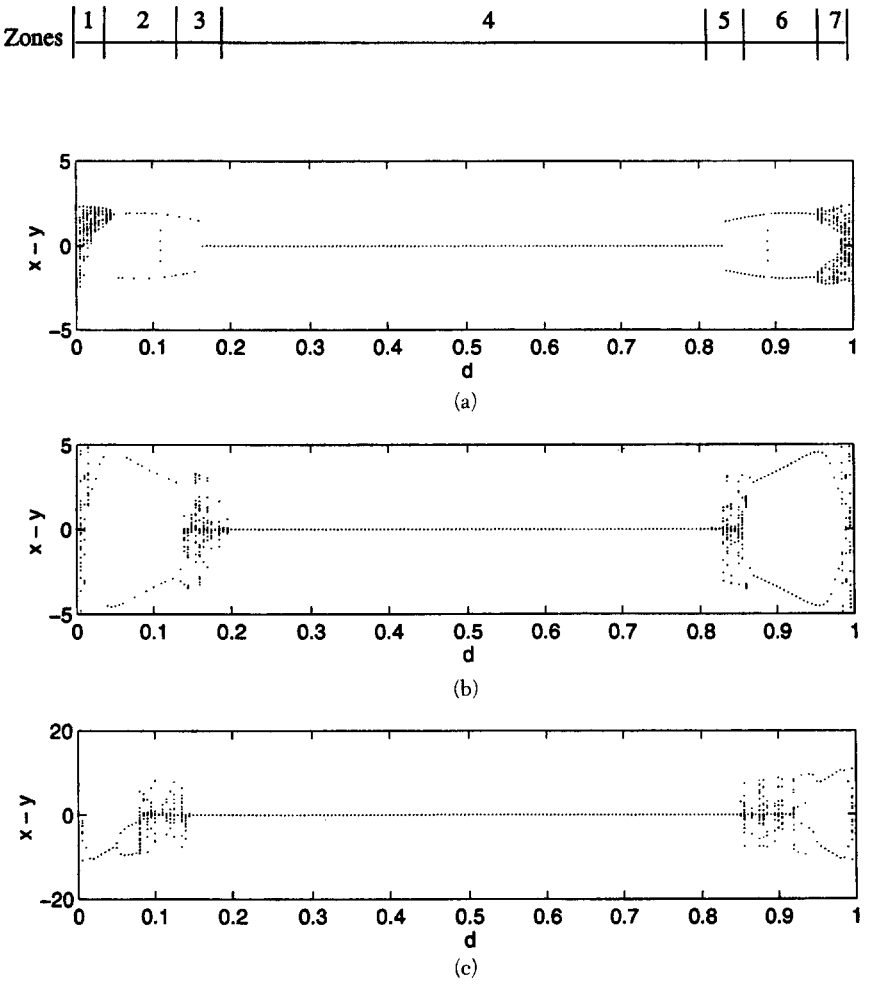

FIG. 9. The difference between x and y plotted against d for three values of r. (a) $\hat{r} = 3$; (b) $\hat{r} = 4$; (c) $\hat{r} = 5$. Synchronicity is observed in zone IV. Such a trend corresponds to a drop in the dimension of the attractor. Zone markings refer to regimes in Figure b. Similar qualitative zones are present for Figures a and c.

n-periodic orbit has two distinct branches and, therefore, the branch the periodic orbits follow may be different depending on the initial conditions.

Consequently, we study the 1-period orbit for different initial conditions. As can be seen from Figure 11, orbits starting from dark regions are attracted to the fixed point located below the diagonal while those starting

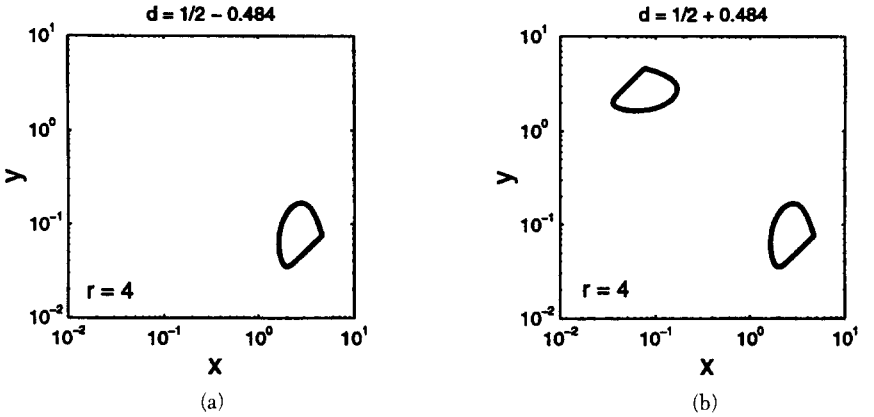

FIG. 10. The transition from zone II to zone I and that from zone VI to zone VII are marked by Hopf bifurcations. (a) The closed loop trajectory caused by the Hopf bifurcation of the one-period orbit in zone II. (b) The closed loop trajectory caused by the Hopf bifurcation of the two-period orbit in zone VI. The orbit alternates between the two closed loops. Further, the two loops are symmetric about the diagonal. $\hat{r} = 4$.

from grey regions are attracted to the fixed point located above the diagonal. These two basins of attraction for the two fixed points are furthermore symmetric about the diagonal. Orbits emanating from near the diagonal (shown in Figure 11 by the small white regions) are attracted to the diagonal. These white regions also possess a symmetry about the diagonal. Overall, though, most of the orbits are attracted to either one of the fixed points while very few are attracted to the chaotic diagonal.

For values of d for which 2-period cycles are observed, similar basins of attraction exist. And orbits emanating from most initial conditions barring a few close to the diagonal appear to be attracted to these 2-period cycles.

In the same way, for values of d in zone IV, trajectories emanating from most initial conditions are attracted to these synchronous orbits as in Figure 12d. However, for values of d in zone III, the trajectories are scattered over a region of the xy-plane (Figure 12a). Thus, the dimension of the chaotic attractor decreases as d is increased from zone III to zone IV.

Notice also that it is possible to have an orbit that is both synchronous and periodic. The fixed point at $(1, 1)$ is a lucid example. This fixed point, however, is unstable for $\hat{r} \geqslant 2$ as demonstrated in the domain-of-stability diagram (Figure 2) and as a result, this synchronous and periodic orbit is not computationally observed.

Over a large range of d the orbits are synchronous (Figure 9). Such a high synchronicity or diagonal attraction is striking. Further, there is also a

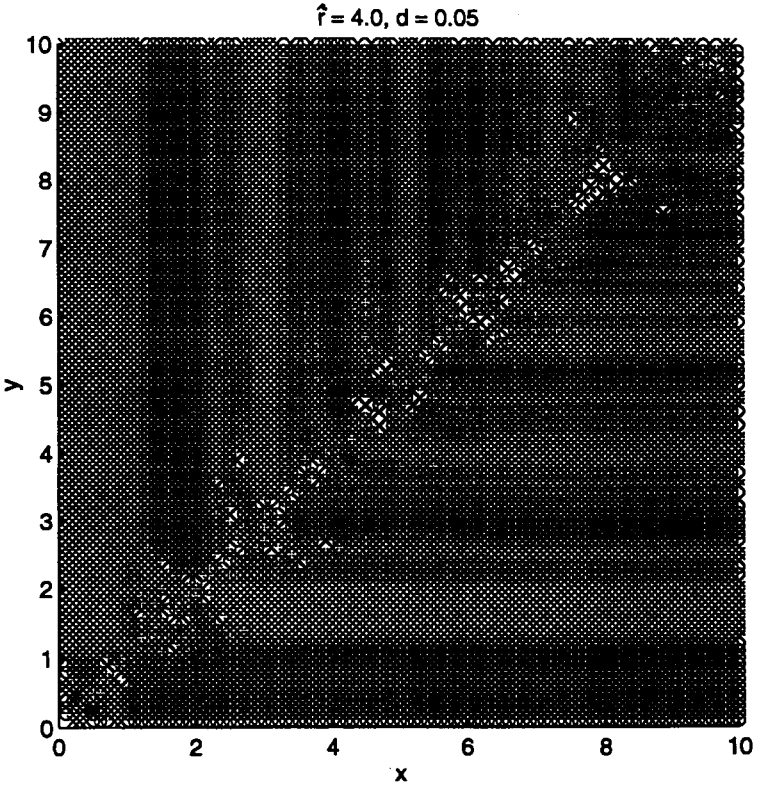

FIG. 11. Basins of attraction for the two fixed points in zone II. The dark regions are attracted to the fixed point below the diagonal ($x = y$), grey regions to the fixed point point above the diagonal and white regions to the chaotic diagonal.

significant range of d over which the dynamical behavior is periodic and one may wonder, given a random coupling (a value of d chosen randomly between 0 and 1), what is the probability of finding periodic or synchronous trajectories. The probability of periodicity, synchronicity, and their total are plotted in Figure 13 for cases in which the base state (state of the underlying single map) is chaotic. For every value of $\hat{r}$ chosen, the probabilities are obtained by investigating the orbits for 5000 values of d ranging from zero to unity. The number of periodic orbits produced divided by 5000 yields the probability of periodic orbits and so on. This procedure is repeated over three initial conditions to obtain an average probability. Because the computational time is high we use only a few different initial conditions. Further, the kinks in the probability of synchronicity are related to the chaotic

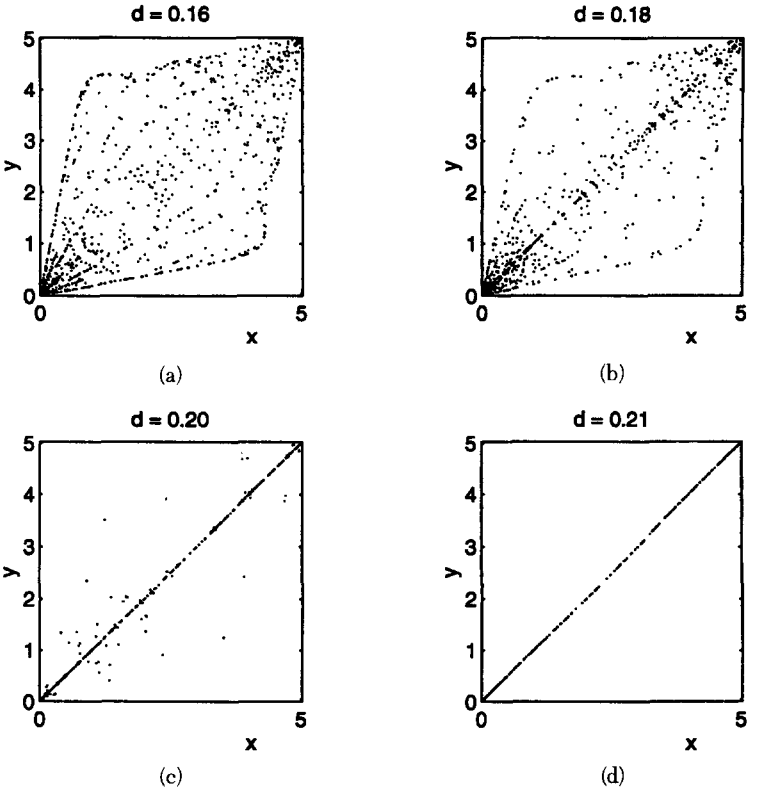

FIG. 12. $\hat{r} = 4$. Plots depicting the diagonal attraction by which orbits emanating from different locations on the $x - y$ plane collapse on to the diagonal. (a) $d = 0.16$; (b) $d = 0.18$; (c) $d = 0.20$; (d) $d = 0.21$.

nature of the trajectories and hence difficult to remove. As $\hat{r}$ is increased from 2.694 to 3.75, the probability of finding periodic orbits increases. But this probability decreases for even higher values of $\hat{r}$. Such a trend is consistent with the periodic orbits of Figures 4–8 where the range of d for periodic orbits increases as $\hat{r}$ is increased from 3 to 4 but decreases as $\hat{r}$ is increased to 5. On the other hand, the probability of synchronicity, on an average, decreases as $\hat{r}$ is increased from 2.694 to about 4.0 but increases for even higher values of $\hat{r}$. These trends are again consistent with those observed in Figure 7. That the probability of finding either a periodic orbit or a synchronous orbit is more than 0.8 indicates that from a probabilistic standpoint, the random coupling of two such chaotic units will most likely result in either a quasi- or complete stabilization.

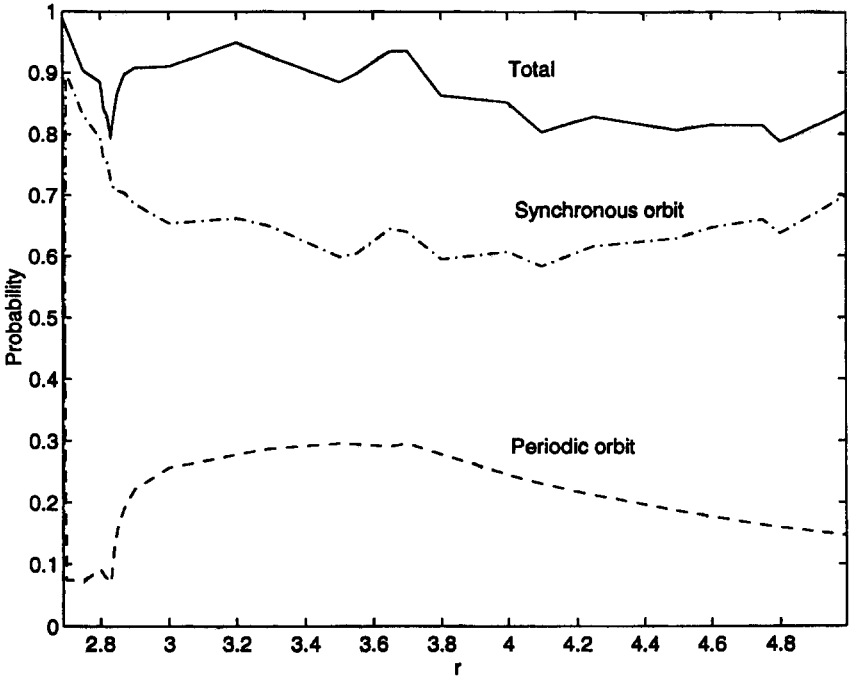

FIG. 13. The probability of obtaining (i) periodic behavior (dashed lines), (ii) synchronous behavior (dash-dot) and (iii) their total, plotted against $\hat{r}$. The probability of finding either periodicity or synchronicity is always more than 0.8.

So far we have considered cases in which the base state (the periodic or chaotic state of the two maps in isolation) is chaotic. And these trends in the probabilities of finding either periodic or synchronous orbits are drastically altered when we change the base state to a periodic state. For values $\hat{r}$ such that the base state is 2^n-periodic i.e., $\hat{r} < 2.694$, the probability of finding a periodic orbit in the coupled system is unity. There are other periodic windows in the single map, for instance, in the vicinity of $\hat{r} = 3.13$ there is a 3-period orbit (Figure 1). The bifurcation plot for the coupled system is shown in Figure 14 for this value of $\hat{r}$.

Again, the dynamical behavior of the coupled system can be categorized into seven zones. In zone I, the 3-period orbit of the base state (or the state of the underlying single map) is reproduced. This is similar to the case of chaotic base state (Figures 4, 5, 9), where zone I was also chaotic. This 3-period orbit in zone I is furthermore synchronous unlike the zone I of the chaotic base state (Figures 4, 5, 9). Zone II is chaotic and asynchronous.

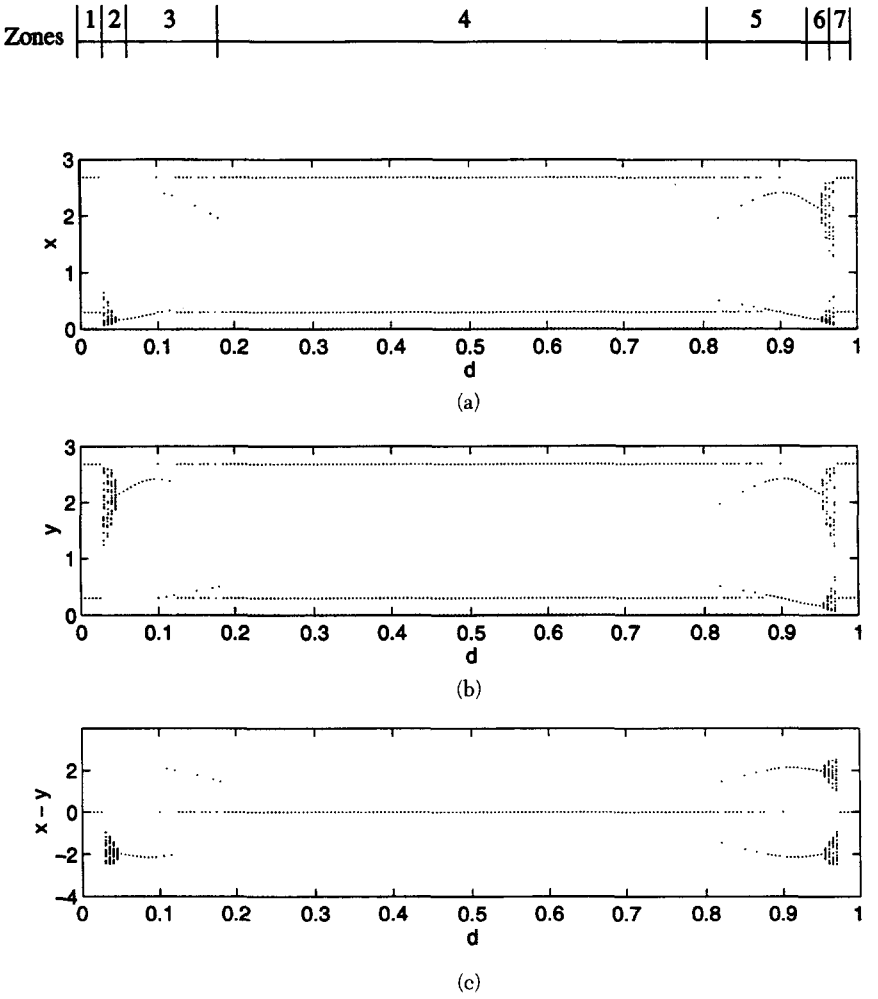

FIG. 14. Behavior of the coupled system when the base state is periodic. For the present value of $\hat{r} = 3.13$, the underlying single map exhibits three-period orbits. Upon coupling two such periodic maps we can obtain chaotic behavior as in zones II and VI. (a) x-ordinate; (b) y-ordinate; (c) $x - y$ plotted as a function of d. Zone markings refer to regimes in all the three subplots.

That coupling two "stable" maps produces chaotic trajectories, is also interesting. Recall that the zone II of the chaotic base state plotted in Figures 4, 5 and 9 was periodic. Therefore, the zone II dynamics is just the opposite of that in the base state. Zone III is periodic and both 1-period and 3-period orbits coexist. Zone IV is characterized by 3-period orbits that are

synchronous. Zones V, VI, and VII are, in agreement with Result 3, similar to zones III, II, and I, respectively.

Thus two conclusions can be arrived at. (i) Whether the dynamics in any zone is periodic or not depends on the base state. If the base state is chaotic and periodic orbits are produced in a particular zone of the coupled system, then chaotic orbits are likely to be produced in the same zone if the base state is periodic and vice versa. (ii) Irrespective of whether the base state is chaotic or periodic, zone IV is always synchronous. The range of d over which the diagonal attracts orbits to produce synchronous orbits is large.

Such a large diagonal attraction is striking and should be analyzed in detail. A coordinate transformation can be used to analyze the global basin of diagonal attraction. Let

$$\xi_n = x_n + y_n; \qquad \eta_n = x_n - y_n.$$

Then, the governing equations (3) reduce to

$$\xi_{n+1} = e^{\hat{r}(1-\xi n/2)}\left[\xi_n \cosh\left(\frac{\hat{r}\eta_n}{2}\right) - \eta_n \sinh\left(\frac{\hat{r}\eta_n}{2}\right)\right]$$

$$\eta_{n+1} = (2d-1)\, e^{\hat{r}(1-\xi n/2)}\left[\eta_n \cosh\left(\frac{\hat{r}\eta_n}{2}\right) - \xi_n \sinh\left(\frac{\hat{r}\eta_n}{2}\right)\right].$$

The diagonal is now given by the equation $\eta = 0$ (or $x = y$). A necessary condition for the diagonal to attract the point (ξ_n, η_n) or (x_n, y_n) is

$$\left|\frac{\eta_{n+1}}{\eta_n}\right| < 1$$

or

$$(2d-1)^2 e^{\hat{r}(2-\xi_n)}\left[\cosh\left(\frac{\hat{r}\eta_n}{2}\right) - \frac{\xi_n}{\eta_n}\sinh\left(\frac{\hat{r}\eta_n}{2}\right)\right]^2 < 1.$$

For orbits starting at a location close to the diagonal such that $x_n = y_0 + \epsilon$ and $y_n = y_0$, the above condition reduces to

$$(1 - \hat{r}y_0)^2(2d-1)^2 \exp(2\hat{r}(1-y_0)) < 1.$$

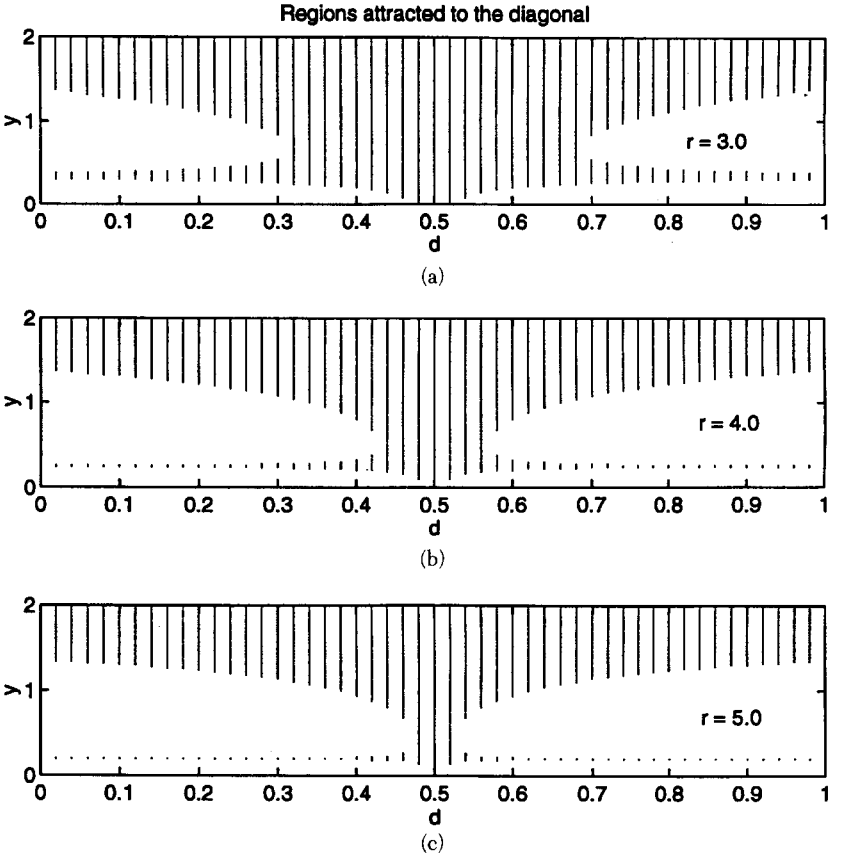

FIG. 15. Regions attracted to the diagonal for different values of $\hat{r}$. (a) $\hat{r} = 3$; (b) $\hat{r} = 4$; (c) $\hat{r} = 5$.

Notice that this condition need *not* be satisfied at each and every point along the line $x = y$. Instead, it is sufficient, if this condition is satisfied on an average along the trajectory traced by the orbit of this map i.e., let us assume that $|\eta_{n+1}/\eta_n| = 1.1$ at the first point of the orbit, the diagonal can still be stable provided at the next point of the orbit $|\eta_{n+2}/\eta_{n+1}| < 1/1.1$. Thus, this synchronicity condition should be satisfied on an average along the entire trajectory.

The values of y_0 for which this condition holds is plotted as a function of the coupling parameter d for three values of $\hat{r}$ in Figure 15. From these plots it is clear that for a given value of d, the range of y_0 satisfying the diagonal attraction condition decreases as $\hat{r}$ is increased. Consequently,

the probability of diagonal attraction should decrease as $\hat{r}$ is increased. On the other hand, from Figure 5 it is clear that as $\hat{r}$ is increased, the orbit reaches larger values of y. This tends to increase the probability of diagonal attraction. Thus we have two competing effects on the probability of diagonal attraction which together produce a minimum probability when $\hat{r} \simeq 4$ as observed in Figure 9.

We next analyze the orbits using Lyapunov exponents. There are two such exponents for this two-dimensional map and both are calculated using the method outlined by Benettin, et al. [13, 14]. Two sets of initial conditions are considered in obtaining these exponents: for one set the initial conditions are not on the diagonal while for the other they are on the diagonal. A typical distribution of the exponents for these two cases is plotted in Figure 16 against d when $\hat{r} = 4$. In both cases, the exponents are symmetric about $d = 1/2$ in agreement with Result 9. Further, in accordance with Result 10, one Lyapunov exponent tends to infinity when $d = 1/2$. When the initial conditions are on the diagonal, the orbit remains on the diagonal (result 4) and chaotic trajectories are generated for all values of d. Consequently, one exponent is always positive. However, when the initial condition is off the diagonal, there are periodic orbits and for the ranges of d in which periodic orbits are found both the Lyapunov exponents are negative. Throughout the chaotic and synchronous regions ($0.2 < d < 0.8$), the larger exponent remains almost a constant with a value of 0.5. The Lyapunov exponents can thus be used to distinguish between periodic and chaotic orbits. However, they cannot be used to distinguish between the different periodic orbits because the values of the exponents characterizing the 1-period orbit for $d = 0.1$ are exactly the same as that characterizing the 2-period orbit for $d = 0.9$. Consequently, one cannot distinguish these two solutions using only the values of the Lyapunov exponents. The Lyapunov exponent plot is enlarged in the range of d for which periodic solutions exist (Figure 17). As d is increased from zero, there is a small range of d in which the two exponents are exactly equal. In this region the 1-period solution has just begun to form and as discussed earlier, the eigenvalues of the Jacobian matrix are complex conjugates. The Lyapunov exponents depend only on the magnitude of the eigenvalues and hence are equal.

3.3. Dynamics and Numerical Results for the Asymmetric Case

Having analyzed the dynamical behavior of the symmetric case, we now focus on the asymmetric case, i.e., $r_x \neq r_y$. We first consider cases in which the asymmetry is very small so that $r_x = r_y + \epsilon$. The values of r_x and r_y are such that both the base states are chaotic.

Again the dynamics is characterized using bifurcation plots that are obtained in the same manner described earlier. The x and y ordinates are

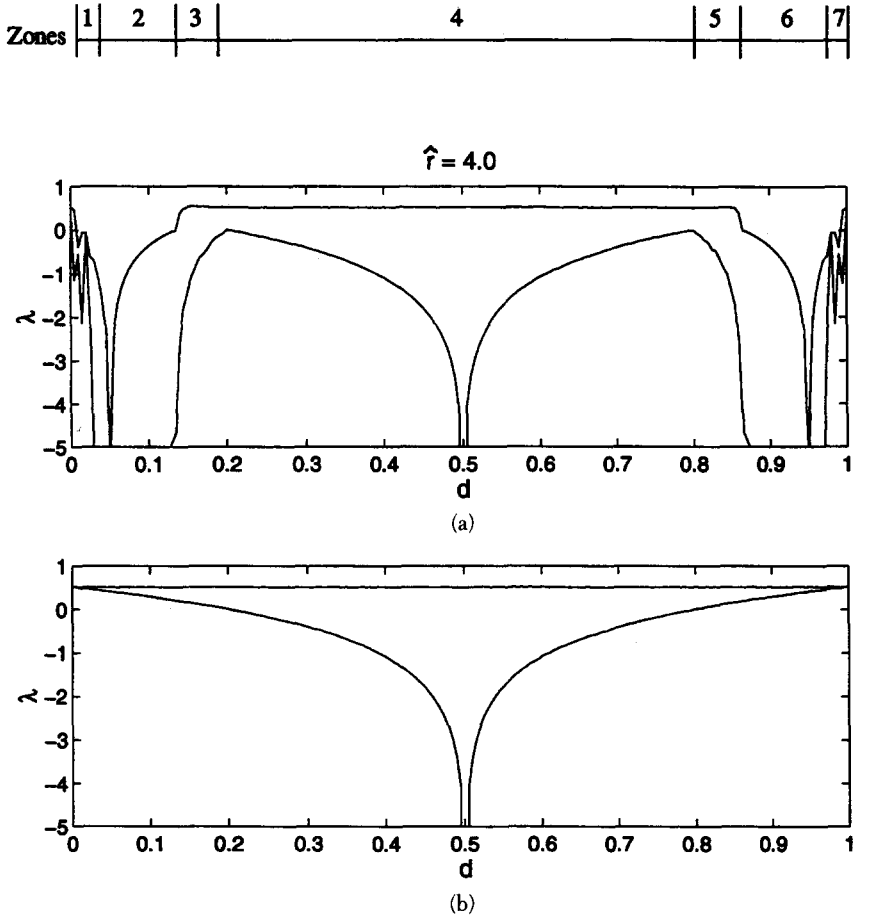

FIG. 16. The spectrum of Lyapunov exponents for different initial conditions. (a) The I.C.s do not fall on the diagonal ($x_0 \neq y_0$). If both the exponents are negative, periodic behavior is observed as in zones II and VI. The values of both the Lyapunov exponents characterizing a one-period orbit in zone II are the same as those characterizing the corresponding two-period orbit in zone VI. Therefore, the spectrum of Lyapunov exponents alone cannot describe the state of the system completely. (b) The I.C.s fall on the diagonal ($x_0 = y_0$). At least one exponent is always positive indicating that the diagonal is chaotic.

plotted in Figures 18 and 19 for three representative values of $r_y (= 3, 4, 5)$. The value of ϵ for all the three cases is 0.1. The overall dynamics of these systems appears very similar to that of the symmetric case.

The global dynamics can be classified again into seven zones marked on Figure 18. These zones are very similar to the corresponding zones for the

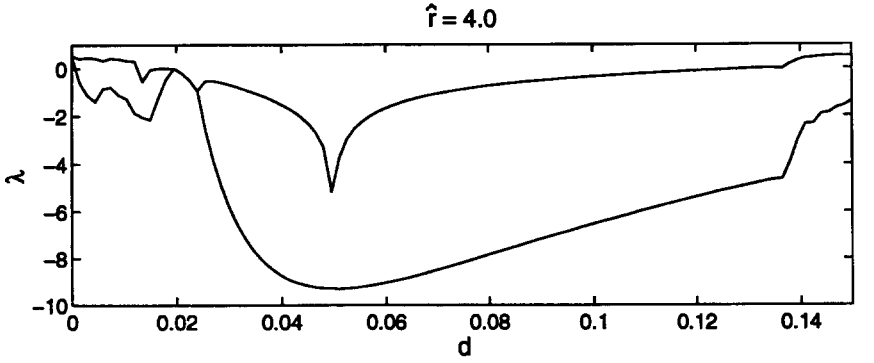

FIG. 17. Enlarged version of Figure 16. Both the exponents are equal at the boundary between zone I and zone II. Recall that the transition from zone II to zone I is via a Hopf bifurcation, and, consequently, the eigenvalues of the Jacobian matrix are complex conjugates. The Lyapunov exponents, being dependent on the absolute value of the eigenvalues, are equal at this boundary.

symmetric case. Zone 1 consists of mostly-chaotic trajectories between which there are several multi-period orbits. Zone II is periodic. This periodic zone exhibits both one-period and two-period orbits. These periodic orbits can be observed in detail by enlarging this zone as in Figure 20. Initially there are two separate one-period trajectories (marked on Figure 20 as A and B) which are nearly but not exactly symmetric about the diagonal $x = y$. In other words, the coordinates of one orbit are almost equal to the transposed coordinates of the other orbit. As d is increased, one of these one-period orbits bifurcates into a two-period orbit. This two-period orbit ceases to exist for larger values of d. Upon further increasing d the second one-period orbit also bifurcates into a two-period orbit.

Zone III is chaotic and there is no visible structure to the trajectories in this region. Zone IV is nearly synchronous, i.e., the value of the x ordinate is nearly the same as that of the y ordinate. Therefore, a plot of $x - y$ should be nearly zero in this region as in Figure 21. Notice that this difference is antisymmetric about $d = 1/2$. In zone 4, the values of this difference for $d = 1/2 - k$ is just the negative of the difference for $d = 1/2 + k$. This anti-symmetry is due to the asymmetry in the growth rates r_x and r_y as explained below.

Assume that at one instant the population at site A (population x_n governed by the growth parameter r_x) is the same as that in site B (population y_n governed by the growth parameter r_y) i.e., $x_n = y_n$. For the next unit of time a specific count of this species is produced at each of the two sites which are then redistributed by the migration parameter d. The

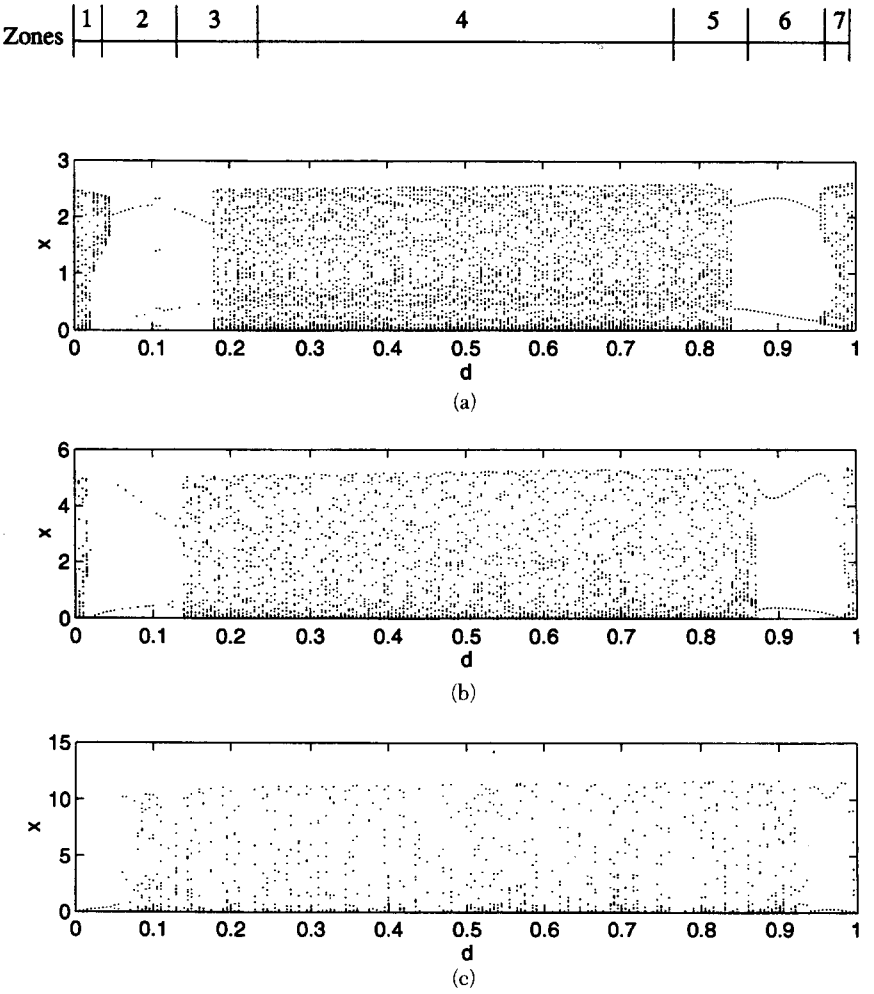

FIG. 18. Asymmetric case. The asymmetry is small such that $r_x = r_y + 0.1$. x-ordinates plotted against d. (a) $r_y = 3$; (b) $r_y = 4$; (c) $r_y = 5$. The trends are similar to the symmetric case Figure 5. Again, there is a significant region of periodic behavior. Zone markings refer to regimes in Figure b. Similar qualitative zones are present for Figures a and c.

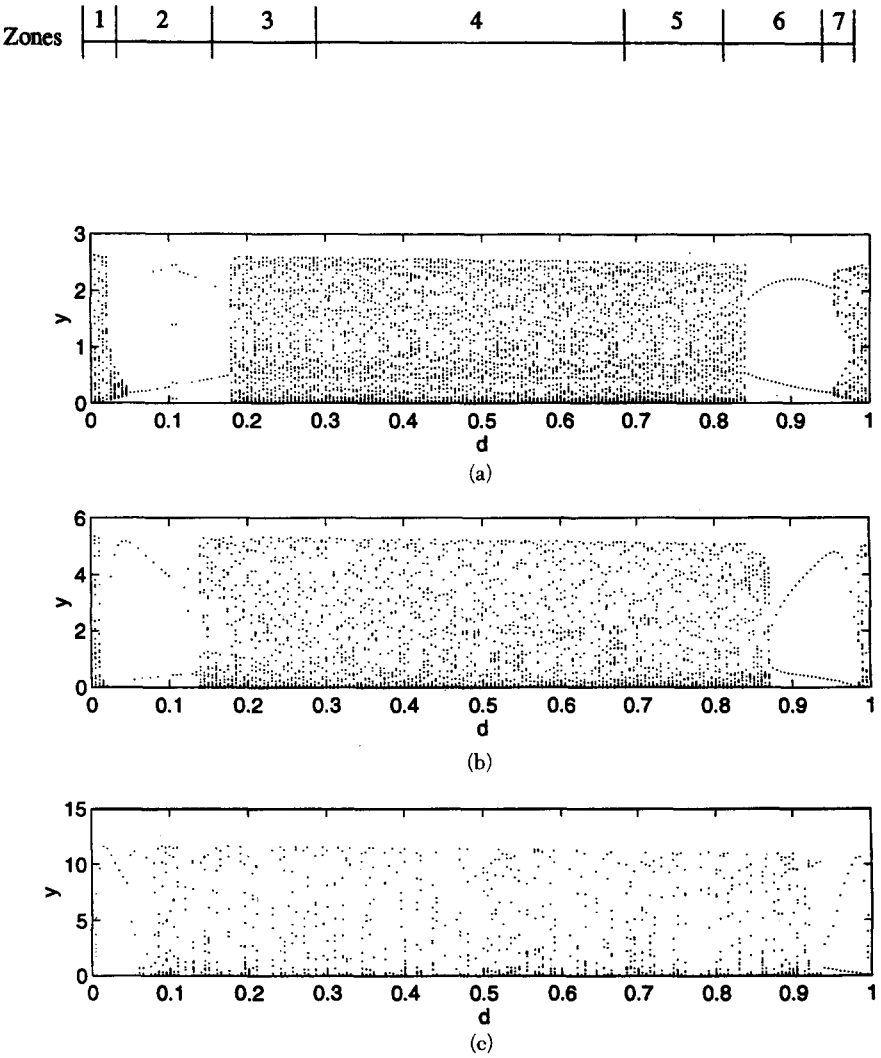

FIG. 19. Asymmetric case. The asymmetry is small such that $r_x = r_y + 0.1$. y-ordinates plotted against d. (a) $r_y = 3$; (b) $r_y = 4$; (c) $r_y = 5$. Zone markings refer to regimes in Figure b. Similar qualitative zones are present for Figures a and c.

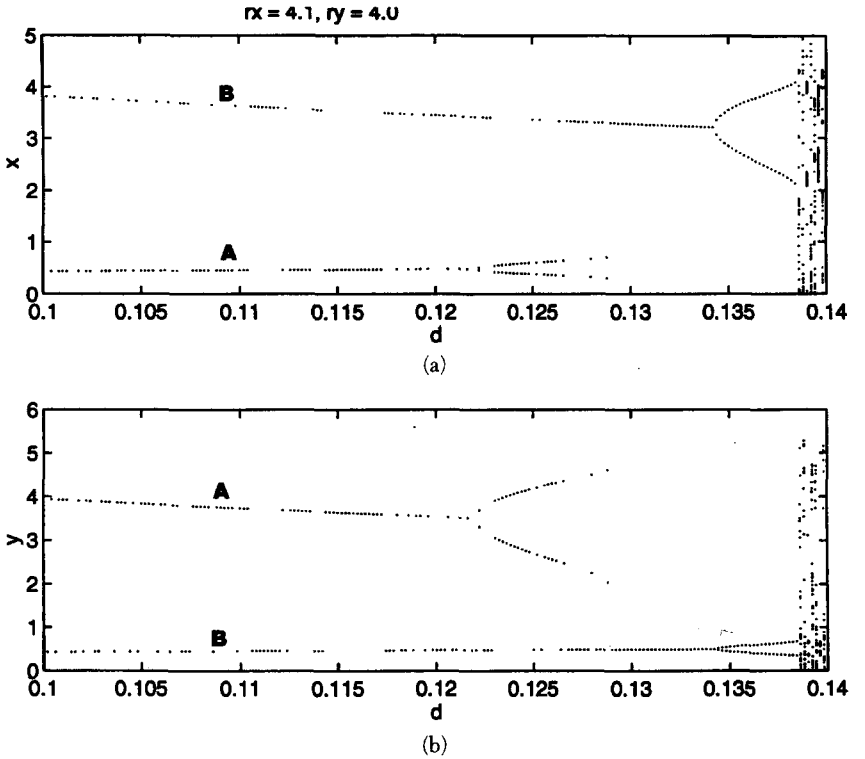

FIG. 20. (a) Zone II of Figure 18b enlarged. (b) Zone II of Figure 19b enlarged. Again the one-period orbits bifurcate into two-period orbits through a pitchfork bifurcation.

amount produced at the first site is

$$P_x = x_n e^{r_x(1-x_n)}.$$

Population produced at the second site is

$$P_y = y_n e^{r_y(1-y_n)} = x_n e^{r_y(1-x_n)}.$$

Now the difference between x_{n+1} and y_{n+1} is

$$x_{n+1} - y_{n+1} = (2d-1)P_x - (2d-1)P_y.$$

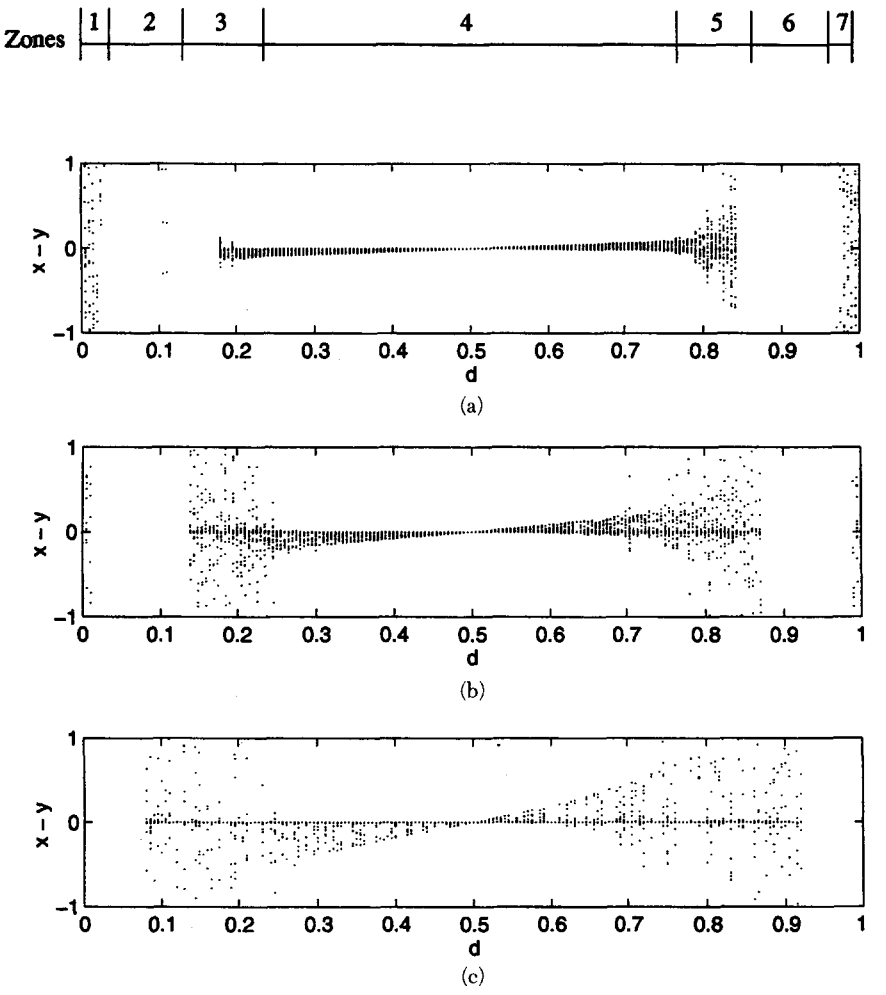

FIG. 21. Asymmetric case. The asymmetry is small such that $r_x = r_y + 0.1$. $x - y$ plotted against d. (a) $r_y = 3$; (b) $r_y = 4$; (c) $r_y = 5$. The synchronicity observed for the symmetric case is broken (compare with Figure 9). Zone markings refer to regimes in Figure b. Similar qualitative zones are present for Figures a and c.

Thus, for $d = 1/2 - k$, the difference $x_{n+1} - y_{n+1}$ is the negative of that for $d = 1/2 + k$, and hence, the anti-symmetry in zone 4 of Figure 21. If the growth parameter r_y is increased from 3 to 5 while maintaining $r_x = r_y + 0.1$, as in Figures 20 and 21, this difference increases because the number produced at each site and their difference increase with r_y.

Zone V, VI, and VII are similar to those of III, II, and I, respectively. The transition from the periodic behavior in zone II to the chaotic behavior in zone I is through a Hopf bifurcation of the one-period orbit. The resulting closed loop trajectory is plotted in Figure 22a. Similarly, the transition from zone VI to zone VII is marked by a Hopf bifurcation of the two-period orbit in zone VI. Such a bifurcation of the two-period orbit leads to two closed loops as in Figure 22b. The orbit alternates between these two loops. Notice that these two loops are not symmetric about the diagonal unlike those in Figure 10.

We next consider cases in which $r_x \ll r_y$. As a typical example we let $r_x = 1.75$ and $r_y = 3$. For $r_x = 1.75$ the base state is periodic with a one-period orbit while for $r_y = 3.0$ the base state is chaotic.

The corresponding bifurcation diagram is depicted in Figure 23. For very small values of d, there is a one period orbit which bifurcates into two, as d is increased to about 0.015. This bifurcation however, does not appear to be a pitchfork bifurcation because we do *not* observe a pitchfork like structure even when the increments of d are reduced to 10^{-7}. Thus, for a certain value of d the one-period orbit loses stability and simultaneously a stable two-period solution appears. This phenomenon has some similarity to the intermittency: in intermittency periodic behavior *suddenly* disappears via a saddle-node bifurcation [11] and chaos results. Here, the one-period orbit bursts *suddenly* into a two-period orbit. This two-period orbit continues to be present for a large range of d and eventually bifurcates into a four-period orbit via a pitchfork bifurcation. This period doubling process, more trans-

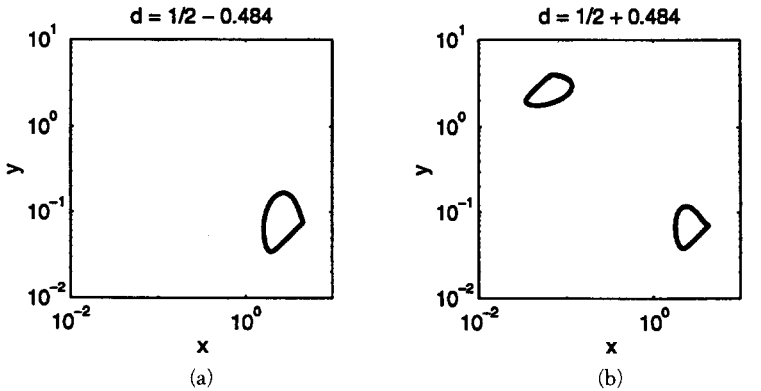

FIG. 22. $r_x = 4.1$; $r_y = 4.0$. (a) Closed loop trajectories obtained at the boundary between zone I and II. (b) Closed loop trajectories obtained at the boundary between zone VI and VII. The two loops are not symmetric about the diagonal (compare with Figure 10).

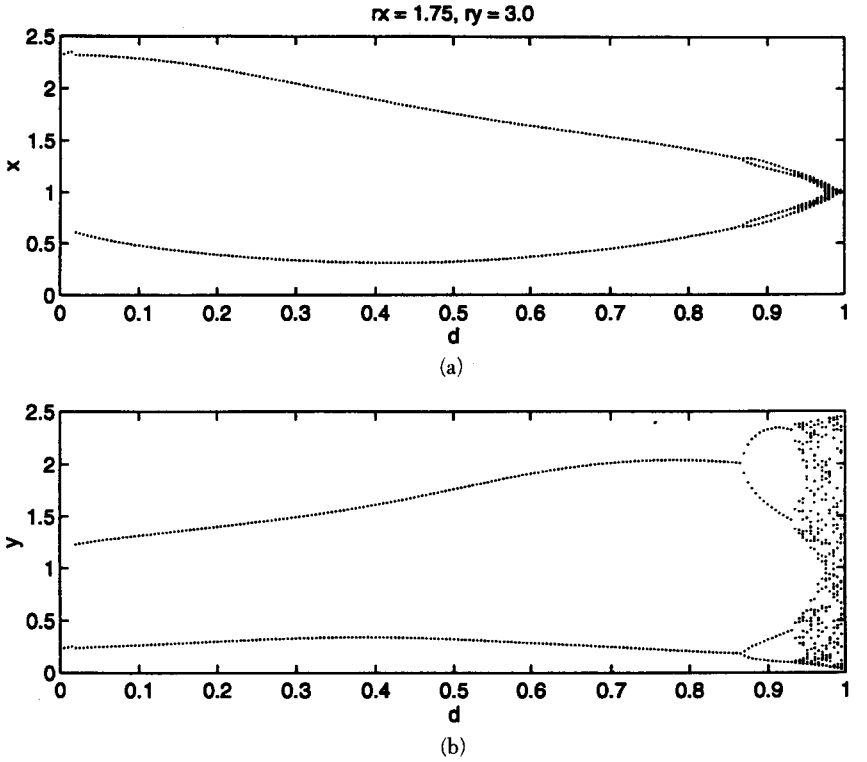

FIG. 23. Asymmetric case. The asymmetry is large such that $r_x = 1.75$ and $r_y = 3.0$. (a) x-ordinate and (b) y-ordinate, plotted against d. For small values of d, there is a one-period orbit which bifurcates into two, as d is increased to about 0.015. But this period-doubling is *not* through a pitchfork bifurcation. The resulting two-period orbit undergoes a series of period-doubling pitchfork bifurcations until the point of accumulation at $d = 0.94078\ldots$.

parent in the enlarged plot of Figure 24, continues until the accumulation point at $d \simeq 0.94078$. Beyond the accumulation point the trajectories are mostly chaotic barring a few periodic windows.

This coupled map also exhibits the same universal constant δ that Feigenbaum [13, 14] has outlined.

$$\delta = \lim_{n\to\infty} \delta_n = \lim_{n\to\infty} \frac{d_n - d_{n+1}}{d_{n+1} - d_{n+2}} \tag{27}$$

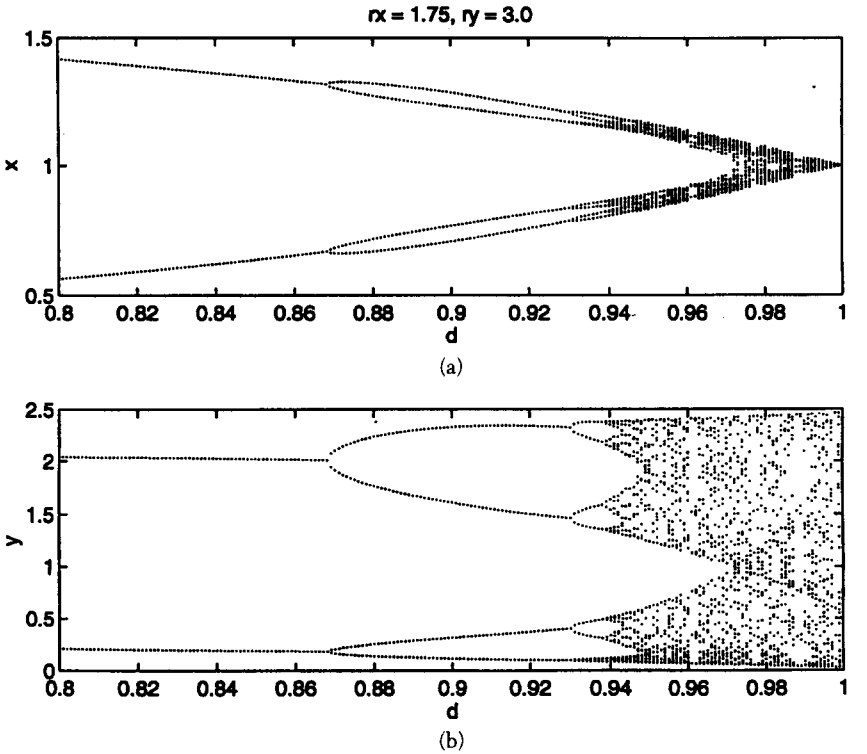

FIG. 24. Enlarged version of Figure 23.

where n stands for the number of period-doubling bifurcations. The values of δ_n, listed in Table 1, indicate that δ_n appears to converge to 4.66902... as $n \to \infty$.

4. DISCUSSION AND APPLICABILITY OF RESULTS TO MORE GENERAL SITUATIONS

It is striking to note that coupling two chaotic systems can produce stable behavior (zone II and VI in plots 5, 6, 18, and 19). In particular, for very high coupling (zone IIA) the trajectories are completely stabilized and stable fixed points are obtained. Thus, migration tends to impose some sort of stability on highly nonlinear systems that are otherwise chaotic. Therefore, coupling the adjacent habitats of a particular species may enhance a

TABLE 1.

n	d_n	δ_n
1	0.01869868	13.695
2	0.8679597	7.157
3	0.9299679	5.056
4	0.9386101	4.721
5	0.9403191	4.641
6	0.940681170	4.644
7	0.940759138	
8	0.940775927	

stable pattern in their population dynamics. Such enhancements may increase the survivability of rare animals as well.

More generally, we have demonstrated that *coupling two chaotic units can indeed stabilize both the units.* Cast differently, a 'jug' of chaos when mixed with another 'jug' of chaos can stabilize both. This stabilizing phenomenon may very well explain why there is so much stability in the physical world despite all the reported chaos. It may therefore be appropriate to *posit a hypothesis that highly nonlinear systems which are chaotic can be stabilized by coupling and that it may be because of the coupling of nonlinear systems in real life that the physical world appears orderly.*

For the case of coupled tent maps Keller et al. [15] have shown that stable 2-period trajectories can be obtained by a suitable coupling of two tent maps that are chaotic but sufficiently close to 2-period motion. We have, on the other hand, demonstrated that periodic trajectories can be obtained by coupling chaotic exponential maps that are far away from periodic behavior.

Coupling two nonlinear units introduces a variety of dynamical behavior into the coupled system. These trends are dependent on the state of the individual nonlinear systems as well as the extent of coupling. The resulting dynamics can broadly be categorized into seven zones as outlined in the previous sections. Further, all the *three* routes to chaos are observed in the present system. Hopf bifurcation route is observed in the transition from zone II to zone I in Figure 5. A phenomenon akin to intermittency is observed in the transition from zone II to zone III. The period-doubling route to chaos is observed in the asymmetric case of Figure 22.

In addition, coupling may also serve as the key to controlling chaos in a wide spectrum of nonlinear phenomena. Coupling can act as a passive control by producing stable behavior as in zones II and VI. Coupling can also be used in active control applications. Recall that coupling produces

unstable fixed points (the dashed line in Figure 3) apart from the stable periodic orbits. Control, based on unstable periodic orbits, is a subject of active recent research [16, 17]. By applying a sequence of small perturbations it is possible to track the unstable periodic orbits.

Our study indicates that bifurcation plots, while extremely useful in analyzing nonlinear systems, should be interpreted with some caution. For a first look, zone IIA of Figure 5 appears to consist of a two-period orbit. Careful observation reveals that it indeed consists of a set of two one-period orbits.

The Lyapunov exponents *cannot* be used to distinguish between the different periodic states because the entire spectrum may be identical for both a one-period orbit (say $d = 0.05$ in Figures 5 and 16) and a two-period orbit (say $d = 0.95$ in Figures 5 and 16).

We have furthermore investigated the symmetry properties present in the system. There is a quasi-symmetry about $d = 1/2$, the effects of which have been analyzed in detail. Further, over a large range of d the diagonal is an attractor when the growth rates of the two adjacent colonies are the same. This diagonal attraction, also termed as synchronicity, may have applications in neuro-biological systems as well. Recent studies indicate synchronized activity in the visual cortex of cats [18] and monkeys [19, 20]. Another study indicates that seizures in rats may be related to bursts of synchronized neural activity in the hippocampus of the rat brain [21]. Understanding synchronized activity is thus important.

It is interesting to note that when the symmetry in the growth rates r_x and r_y is altered slightly, the synchronicity is also altered slightly. Thus, the match of a system parameter such as the growth parameter may be the key to understanding synchronicity.

There are some limitations to the coupling used in this study. First the coupling is symmetric, i.e., the percentage of organisms migrating from colony A to colony B is the same as that migrating from colony B to colony A. But in reality, migration is asymmetric with more organisms migrating to the better habitat, say the habitat that has more food. Second, there is always a threshold of population beyond which migration can take place. That is, the coupling parameter d should depend on the population levels x and y. Migration of human beings into the United States is a lucid example in this regard. This migration is often higher for people coming from regions that are densely populated. We have ignored such effects to keep the system simple.

Further, instead of just two populations interacting with each other, there may be several populations interacting with each other. Such systems may also exhibit pattern formations observed in other spatially-extended physical systems such as Rayleigh-Benárd convection [24]. In such cases,

several additional questions arise. How many stable systems are required to stabilize the entire system? How should they be distributed? For example, if we were to consider a ring of neurons, how many stable neurons should be present on this ring? Where should these stable neurons be located so that we can stabilize the entire system? How does the number of required stable neurons depend upon their locations? Further research along the lines described in this paper may provide the answers to some of these questions.

REFERENCES

1 I. Hanski, Single-species metapopulation dynamics: concepts, models, and observations, in (M. E. Gilpin and I. Hanski, eds.), *Metapopulation Dynamics*, Academic, London, 1991.

2 W. E. Ricker, Stock and recruitment, *J. Fish. Res. Board. Canada*, 11:559 (1954).

3 R. M. May, Simple mathematical models with very complicated dynamics, *Nature*, 261:459 (1976).

4 M. Gyllenberg, G. Soderbacka, and S. Ericsson, Does migration stabilize local population dynamics? Analysis of a discrete metapopulation model, *Mathematical Biosciences*, 118:25 (1992).

5 R. A. Chowdhury, and K. Chowdhury, Bifurcations in a coupled logistic map, *International Journal of Theoretical Physics*, 30:97 (1991).

6 K. Kaneko, Transition from torus to chaos accompanied by frequency lockings with symmetry breaking, *Progress in Theoretical Physics*, 69:1427 (1983).

7 H. Fujisaka, and T. Yamada, Stability theory of synchronized motion, *Progress of Theoretical Physics*, 69:32 (1982).

8 H. G. Schuster, S. Martin, and W. Martienssen, New method for determining the largest Lyapunov exponent of simple nonlinear systems, *Physical Review A*, 33:3347 (1986).

9 P. Pikovsky, A. S. Grassberger, Symmetry breaking bifurcation for coupled attractors, *Journal of Physics, A*, 24:4587 (1991).

10 D. Ruelle, and F. Takens, On the nature of turbulence, *Commun. Math. Phys.*, 20:167 (1971).

11 Y. Pomeau, and P. Manneville, Intermittent transition to turbulence in dissipative dynamical systems, *Commun. Math. Phys.* 74:189 (1980).

12 F. E. Udwadia, and R. S. Guttalu, Chaotic dynamics of a piecewise cubic map, *Physical Review A*, 40:4032 (1989).

13 M. J. Feigenbaum, Quantitative universality for a class of nonlinear transformations, *J. Stat. Phys.* 19:25 (1978).

14 G. Bennetin, L. Galgani, and J. M. Strelcyn, The Lyapunov characteristic exponents for a smooth dynamical system and for hamiltonian systems; a method for computing all of them. Part 2: Numerical application, *Meccanica*, 15:21 (1980).

15 G. Keller, M. Kunzle, and T. Nowicki, Some phase transitions in coupled map lattices, *Physica D*, 59:39 (1992).

16 E. Ott, C. Grebogi, and J. A. Yorke, *Physical Review Letters*, 64:1996 (1990).
17 U. Dressler, T. Ritz, A. S. Z. Schweinsberg, R. Doerner, B. Hubinger, and W. Martienssen, Tracking unstable periodic-orbits in a bronze ribbon experiment, *Physical Review E*, 51:1845 (1995).
18 A. Engel, P. Konig, A. Kreiter, T. Schillen, and W. Singer. Temporal coding in the visual cortex: new vistas on integration in the nervous system. *Trends Neurosci.*, 15:218 (1992).
19 A. K. Kreiter, and W. Singer, Oscillatory neuronal responses in the visual cortex of the awake monkey, *Eur. J. Neurosci.*, 4:369 (1992).
20 M. S. Livingston, Visually-evoked oscillations in money striate cortex, *Soc. Neurosci. Abstr.*, 17:73.3 (1991).
21 S. J. Schiff, K. Jerger, D. H. Duong, T. Chang, M. Spano, and W. L. Ditto, Controlling chaos in the brain, *Nature*, 370:615 (1994).
22 G. Bennetin, L. Galgani, and J. M. Strelcyn, The Lyapunov characteristic exponents for a smooth dynamical systems and for hamiltonian systems; a method for computing all of them. Part 1: Theory, *Meccanica* 15:9 (1980).
23 M. J. Feigenbaum, The universal metric properties of nonlinear transformations, *J. Stat. Phys.*, 21:669 (1979).
24 T. Yanagita and K. Kaneko, Rayleigh-Benard Convection—patterns, chaos, spatiotemporal chaos and turbulence, *Physica D* 82:288 (1995).